AD-A177 576 OPTICAL PROBING OF ACOUSTIC EMISSION DURING DEFORMATION OF MICROTENSILE SPECIMENS(U) ARMY BALLISTIC RESEARCH LAB ABERDEEN PROVING GROUND MD W J BRUCHEY DEC 86 BRL-TR-2774 1/1

UNCLASSIFIED F/G 20/11 NL

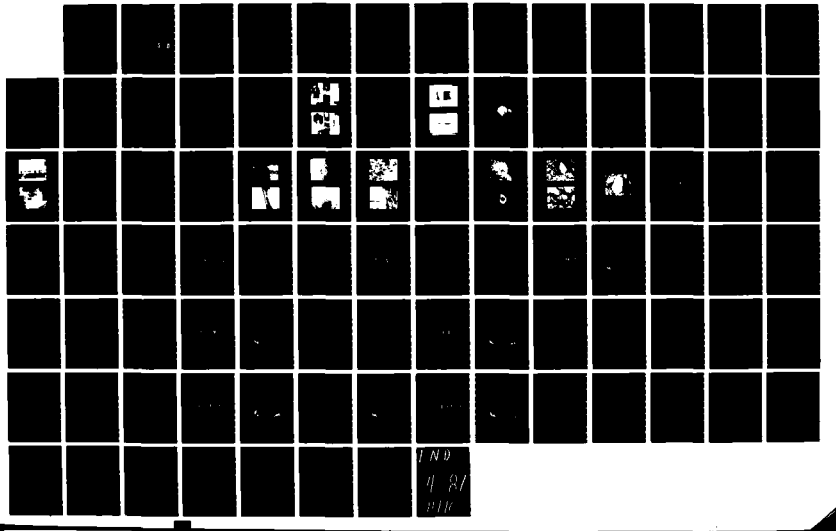

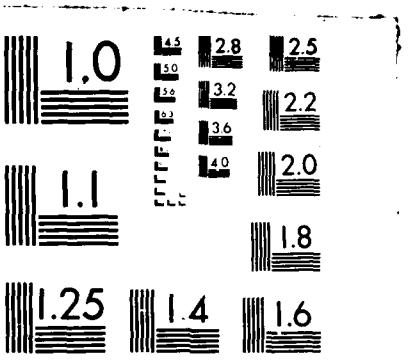

MICROCOPY RESOLUTION TEST CHART
NATIONAL BUREAU OF STANDARDS-1963-A

AD-A177 576

COPY OF COPIES, SERIES A

AD

(12)

TECHNICAL REPORT BRL-TR-2774

OPTICAL PROBING OF ACOUSTIC EMISSION DURING DEFORMATION OF MICROTENSILE SPECIMENS

WILLIAM J. BRUCHEY, JR.

DTIC ELECTE MAR 0 3 1987 S D

DECEMBER 1986

DTIC FILE COPY

APPROVED FOR PUBLIC RELEASE; DISTRIBUTION UNLIMITED.

US ARMY BALLISTIC RESEARCH LABORATORY
ABERDEEN PROVING GROUND, MARYLAND 21005-5066

87 3 2 007

Destroy this report when it is no longer needed.
Do not return it to the originator.

Additional copies of this report may be obtained from the National Technical Information Service, U. S. Department of Commerce, Springfield, Virginia 22161.

The findings in this report are not to be construed as an official Department of the Army position, unless so designated by other authorized documents.

The use of trade names or manufacturers' names in this report does not constitute indorsement of any commercial product.

UNCLASSIFIED

SECURITY CLASSIFICATION OF THIS PAGE (When Data Entered)

REPORT DOCUMENTATION PAGE		READ INSTRUCTIONS BEFORE COMPLETING FORM
1. REPORT NUMBER	2. GOVT ACCESSION NO.	3. RECIPIENT'S CATALOG NUMBER
4. TITLE (and Subtitle) Optical Probing of Acoustic Emission During Deformation of Microtensile Specimens		5. TYPE OF REPORT & PERIOD COVERED 6. PERFORMING ORG. REPORT NUMBER
7. AUTHOR(s) William J. Bruchey, Jr.		8. CONTRACT OR GRANT NUMBER(s) 1L161101A91A
9. PERFORMING ORGANIZATION NAME AND ADDRESS U.S. Army Ballistic Research Laboratory ATTN: SLCBR-TB Aberdeen Proving Ground, MD 21005-5066		10. PROGRAM ELEMENT, PROJECT, TASK AREA & WORK UNIT NUMBERS
11. CONTROLLING OFFICE NAME AND ADDRESS U.S. Army Ballistic Research Laboratory ATTN: SLCBR-DD-T Aberdeen Proving Ground, MD 21005-5066		12. REPORT DATE 13. NUMBER OF PAGES 89
14. MONITORING AGENCY NAME & ADDRESS(if different from Controlling Office)		15. SECURITY CLASS. (of this report) Unclassified 15a. DECLASSIFICATION/DOWNGRADING SCHEDULE

16. DISTRIBUTION STATEMENT (of this Report)

Approved for public release; distribution unlimited.

17. DISTRIBUTION STATEMENT (of the abstract entered in Block 20, if different from Report)

18. SUPPLEMENTARY NOTES

19. KEY WORDS (Continue on reverse side if necessary and identify by block number)

Acoustic Emission	Non-Destructive Testing
Stainless Steel	Failure
Fracture	Materials

20. ABSTRACT (Continue on reverse side if necessary and identify by block number)

Optical interferometric techniques were adapted to detect and analyze acoustic emission signals from 304L stainless steel. The objective of this study was to determine the correlation between fracture surface topography and acoustic emission signals emitted by the material during plastic deformation and failure, and to reconcile this information with existing theories of acoustic emission generation in polycrystalline materials. A pneumatic load system was developed to accept an optical interferometer as the device for detecting

DD FORM 1 JAN 73 1473 EDITION OF 1 NOV 65 IS OBSOLETE

UNCLASSIFIED

SECURITY CLASSIFICATION OF THIS PAGE (When Data Entered)

ABSTRACT

cont'd

acoustic emission signals. Microtensile specimens were fabricated which limited the zone of deformation to approximately three cubic millimeters in volume. Use of the optical probe permitted the monitoring of transient surface displacements at locations within fractures of a millimeter of the deforming volume. Results demonstrate that acoustic emission is a volume phenomena. For the small plastic zone size investigated, the acoustic emission counts have been minimized to the extent that signals are separated in time and waveform analysis can be conducted on each of the signals. Test results show that models describing dislocations as the source of acoustic emission are not sufficient to describe the observed behavior. (keywords!)

TABLE OF CONTENTS

Accesion For
NTIS CRA&I ☑
DTIC TAB ☐
Unannounced ☐
Justification
By
Distribution/
Availability Codes
Dist | Avail and/or Special
A-1

DTIC COPY INSPECTED 6

LIST OF ILLUSTRATIONS

LIST OF ILLUSTRATIONS (cont)

LIST OF ILLUSTRATIONS (cont)

LIST OF ILLUSTRATIONS (cont)

I. INTRODUCTION

During the deformation and ultimate failure of crystalline materials due to imposed loads, the elastic strain energy stored within the material or structure can be released in a number of ways. One form in which this energy release phenomena manifests itself is as elastic waves which radiate from regions of rapid strain relaxation. When these elastic waves reach the surface of the body they cause displacements that can be detected by various types of sensors and are termed acoustic emissions.

Kaiser is credited with the first serious work in the field of acoustic emission.[1] He conducted studies on polycrystalline zinc, steel, aluminum, copper and lead. Emissions were found in all the materials studied and Kaiser presumed that grain boundary motion induced by the applied stress was the source of the emissions. While this hypothesis has since been discounted, Kaiser did definitively demonstrate that acoustic emission is intimately related to deformation processes. Schofield conducted subsequent experiments and expanded the work of Kaiser. His prime purpose was to determine the source of the emissions and his single crystal work showed conclusively that grain boundary effects were not the only source of emissions. Schofield was the first to make a real distinction between burst type (discrete) and continuous type emissions.[2] [3]

As the name implies, continuous type emissions are the component of the acoustic signal occurring sufficiently often during deformation to be regarded as continuous. It has been generally associated with plastic deformation occurring at relatively small plastic strains.[4] It increases in amplitude as the load is applied during a tensile test and appears as an increase in the noise level. Researchers have shown a decrease in this component with increasing strain after yield.

The second component of the acoustic emission signal does not occur continuously but in bursts.[4] It is usually of higher amplitude than the continuous component.

There are a number of excellent review articles describing the gamut of scientific investigations conducted and the technological applications of the

---

[1] *J. Kaiser, PhD. Thesis, Tech. Hochsch., Munchen (1950).*

[2] *B. H. Schofield, AF 33(616)-5640, Lessells and Associates, Inc., Boston, 1960.*

[3] *B. H. Schofield, Proc. of Symposium on Physics and Non-Destructive Testing, 63-82, 1963.*

[4] *R. G. Liptai, D. O. Harris, R. B. Engle, C. A. Tatro, Int. J. of NDT, Vol. 3, 215-275, 1971.*

phenomena spanning more than 20 years work.[5-12] Acoustic emission has had the distinction of being employed extensively in the field of non-destructive testing to confirm that structures or components are fit for use. Yet, its utility as a non-destructive test tool is often over-shadowed by a lack of knowledge as to the underlying mechanisms producing the signals. Many mechanisms have been offered as possible sources, some of the principles ones are:[13]

- Twinning
- Phase transformations
- Mobile dislocation motion
- Grain boundary sliding
- Slip band formation
- Dislocation unpinning
- Plastic deformation at a stress concentration
- Void initiation
- Crack growth
- Fracture of inclusions and second phase particles

---

[5] *H. L. Dunegan, A. S. Tetleman, Research/Development, May 1971, p. 20.*

[6] *A. E. Lord, "Physical Acoustics," W. P. Mason and R. N. Thurston (Editors), Vol. 11, p. 289, 1975.*

[7] *A. A. Pollack, Acoustics and Vibration Progress, R. W. B. Stephens and H. G. Leventhall (Editors), Vol. 1, p. 53-84, 1974.*

[8] *P. H. Hutton, R. N. Ord., "Acoustic Emission", R. S. Sharpe (Editor), Research Techniques in NDT, P. 1-30, 1970.*

[9] *R. G. Liptai, D. O. Harris, C. A. Tatro (Editors), ASTM STP 505, ASTM, Phila., Pa., 1972.*

[10] *J. C. Spanner, Acoustic Emission, Techniques and Applications, INTEX Publ. Co., Evanston, Ill., 1974.*

[11] *A. E. Lord, Physical Acoustics, W. P. Mason and R. N. Thurston (Editors), Vol. 11, p. 289, 1975.*

[12] *J. C. Spanner, J. W. McElroy (Editors), Monitoring Structural Integrity by Acoustic Emission, ASTM STP 571, ASTM, 1975.*

[13] *M. Arrington, British J. of NDT, 17, p. 10, 1975.*

Several different techniques are available to the researcher to characterize recorded events. These are:[13]

- Event Counting - This is the simplest measure of emission activity where each emission contributes one count irrespective of the magnitude of the event. The greatest shortcomings of this technique are the assumption that all events are equally damaging to the structure, that all damaging events will produce acoustic emissions of sufficient amplitude to be counted, and that each event will cause an acoustic emission which will be counted only once and not overlap with other signals.

- Amplitude Sorting - Each emission is characterized by the amplitude of its largest cycle. These amplitudes are then sorted into ranges typically 2-20 db wide. This technique, a modification of event counting, suffers from the same deficiencies as event counting.

- Threshold Crossing - The importance of an emission is characterized by the number of times the ring-down counts trigger a preset threshold. This gives an indication of the energy contained in the stress wave. The difficulty with this approach is that a structurally damaging event may occur but the emissions associated with it may be too weak to cross the threshold or propagate away from the detecting transducer or even be of the wrong frequency to be detected.

- Event Characterization - Or waveform analysis has the greatest potential of exposing the mechanisms of acoustic emission. However, this potential is difficult to exploit because of a lack of broadband equipment capable of capturing acoustic waveforms without altering the characteristic frequency spectra of the source.

In recent years, increased attention is being given to the correlation of microstructural changes to acoustic emission response. However, in many cases direct metallographic or other independent evidence was not presented to verify microstructural features as the source of acoustic emission. This statement is not meant to fault those investigators. The interaction or accommodation required between instrumentation limitations and material sample size (i.e. dimensional restrictions) force the experimenter to compromise his desire to conduct the most definitive test with his ability to gather valid data.

This restriction on running the "ideal" test has been caused in the past by available instrumentation. The piezoelectric transducer has been the primary means of gathering acoustic emission information. Seeking to make the specimen small to eliminate selected filtering of the waveform by the specimen itself results in problems of transducer response. This is because an acoustic emission source has a small extension in space. If the transducer were essentially placed in contact with it, the transducer would respond abnormally. Reliable representation of a signal by the transducer assumes that the stress acting over the sensitive face of the transducer is uniform. That is, it is assumed that the transducer is excited in a one-dimensional stress mode. If the transducer is excited only over a small region of its sensitive face, it will be operating in a more complicated stress mode.[4] Additionally, with these type sensors the problem of waveform modification results from the use

of an acoustic couplant as a transfer medium for transferring the specimen surface displacements to the sensitive area of the transducer.

Of particular interest for frequency analysis of the acoustic emission waveform is the resonant nature of the piezoelectric transducer. No matter how well damped, the frequency response will not be flat but exhibit regimes of variable frequency sensitivity.

In recent years, flat frequency response sensors have come into use. These sensors eliminate two of the more serious deficiencies of the piezoelectric types: (1) Non-uniform frequency response, and (2) direct contact of the sensor with the specimen surface. These sensors fall into two categories: (1) Air gap capacitance, and (2) optical interferometer.

The air gap capacitance transducer is non-contact and exhibits a flat frequency response.[14] Its biggest shortcoming is a lack of sensitivity relative to the piezoelectric type. Consequently, its use has been limited to the characterization of the more energetic events. While its response may be true, it does effectively filter out certain waveforms. Since source identification is often inferred from models of deformation processes or after the fact examination of the failed specimen, the fact that certain waveforms may not be represented may make the matching of signal to source difficult or impossible.

The last method of sensing acoustic emission signals to be discussed is the optical method. The adaption of optical interferometry to the detection and characterization of acoustic emission waves has been recently accomplished.[15-18] The important advantage of the optical detector, as with the capacitance sensors, is no direct contact with the specimen, very broad flat frequency response and no requirement for an impedance matching couplant. Over and above the piezoelectric and capacitance sensors, the optical detector is free from mechanical resonances; can be absolutely calibrated; can probe internally in transparent media; and, can be used over a wide temperature range and in hostile environments. Since the focused beam of the interferometer can be typically only a few hundredths of a millimeter, it can be used to probe very close to twins, slip bands, cracks or other defects. For this reason, it is more accurately referred to as an optical probe.

As stated previously, the acoustic emission event is essentially a point source phenomena. Its amplitude decreases with increasing distance from the source due to simple geometric considerations of an expanding wavefront and as a result of various energy loss mechanisms such as thermoelastic effects, grain boundary scattering, acoustic diffraction, dislocation damping, interaction

---

[14] *H. N. G. Wadley, C. B. Scruley, Acta. Met., Vol. 27, p. 623, 1979.*

[15] *S. E. Fick, C. H. Palmer, Applied Optics, Vol. 17, No. 17, p. 2686, 1978.*

[16] *R. A. Kline, R. E. Green, C. H. Palmer, J. Acoust. Soc. Am., 64(6), 1978.*

[17] *C. H. Palmer, S. E. Fick, Proc. of Southeastcon '79, p. 191, 1979.*

[18] *C. H. Palmer, R. E. Green, "Optical Probing of Acoustic Emission Waves," Final Report, U.S. Army Research Office, North Carolina, 1979.*

with ferromagnetic domain walls and scattering due to point defects. In practice, one also finds that acoustic emission sources produce signals composed not of a single frequency and amplitude but, rather, of a spectrum of frequencies and amplitudes. To properly characterize the signals this entire spectrum should be detected. Each of the above loss mechanisms attenuates the higher frequency signals more than the lower frequency components. Consequently, the sensor must possess flat frequency response and high sensitivity. These are met with the optical detector.

Many factors effect the frequency and amplitude distribution of the recorded signal and it is highly desirable that the detector be situated as close as possible to the source. By localizing the volume of plastically deforming material sufficiently, the sensor will be in close proximity to the source. As described later, the tensile specimen geometry chosen limits the deformation to a rectangular volume of approximately three cubic millimeters. The optical probe with a focused beam diameter of fractions of a millimeter is ideally suited for probing immediately adjacent to this volume. For all these reasons, the optical probe was the sensor of choice.

As previously mentioned, two factors limit the information that is present or can be extracted from the waveform. The use of the optical probe addresses the extraction of information. The loss mechanisms within the material itself account for the loss of information in the waveform. These mechanisms can never be eliminated because no material can ever be the ideal linear elastic homogeneous isotropic solid of continuum mechanics. However, it is possible to minimize these effects. Schofield was the first to show that acoustic emission is a volume phenomena[3] James and Carpenter[19] showed that acoustic *emission count rate* is proportional to the volume of the deforming specimen. Reducing the size of the gage volume would offer the following advantages:

- Reduce the number of potential loss or attenuation sites present;
- Allow placement of the sensor close to the source;
- Reduce the number of potential sites for acoustic emission generation;
- Reduce the overlap between signals since fewer will be generated.

The microtensile specimen in concert with the optical probe has the potential to exploit these advantages.

II. EXPERIMENTAL CONSIDERATIONS

The primary goal of this study was to employ a unique detection system and specimen geometry in an attempt to identify and characterize the sources of acoustic emission. The acoustic emission investigator operates in much the same manner as the forensic scientist in a criminal investigation. He is presented with a corpse with a bullet hole in it. He is then asked to identify the bullet that made the hole; the cartridge it was fired from; the gun used

---

[19] *D. R. James, S. H. Carpenter, Scripta Met., Vol. 10, p. 779, 1976.*

to fire the cartridge; and who was holding the gun when it was fired. To be successful in his investigation, he would like to have as few different paths as possible to follow from the bullet hole to the killer. In a sense, the efforts taken in this study were pointed towards limiting the number of possible suspects who could have committed the crime to minimize the number of paths one could take to get from the bullet hole to the killer.

To this end, the acoustic emission investigator would like:

1. The spectrum of possible sources to be as limited as possible,

2. As accurate a description of the signature of the acoustic event as modern instrumentation allows,

3. The events to be spread out in either time or space to minimize the overlapping of events and increase the likelihood of obtaining a true signature of the event.

A. Material Selection.

A judicious choice of the material investigated provided the desirable characteristic of limiting the potential sources of acoustic emission. A full spectrum of choices was available all the way from single crystals up through complicated engineering alloys. It was decided that an engineering alloy should be chosen since the ultimate goal of acoustic emission is to inspect engineering structures under service conditions. The alloy chosen was 304L stainless steel.[20]

This material falls within the general category of an austenitic stainless steel. These stainless alloys enjoy the greatest usage of all the stainless steels. They are characterized by a low yield strength, excellent ductility and relatively high ultimate tensile strength at room temperature. They are not hardenable by heat-treatment but harden to a degree when cold worked. Type 304L stainless steel, in particular, was developed with a low carbon content to minimize the formation of chromium carbides at the grain boundaries. Segregation of the Cr_2C particles at the grain boundaries was found to be deleterious when the material was welded and reduced its resistance to intergranular attack in corroding media. Its nominal composition is:

C	Cr	Ni	Mn	Si,max	Pmax	Smax
0.03 max	18.00-20.00	8.00-12.00	2.00 max	1.00	0.045	0.030 .

To meet the goal of minimizing the possible sources of acoustic emission, 304L is single phase (metastable austenite) and contains a limited number of hard carbide particles located at or near the grain boundaries. Microstructural interpretation of the sources of the acoustic emission signals from this material are, therefore, not complicated by multi-phases, in which any of the phases can be a source of noise, nor by a number of different intermetallic inclusions highly dispersed throughout the matrix.

---

[20] *W. C. Rion, "Stainless Steel Information Manual for the Savannah River Plant," Vol. 1, Dupont Report DP-860, 1964.*

Not only do the above features of 304L limit the potential sources, they also contribute to the third of our "likes" list: Limiting the sources should also contribute to spreading out the events in time or space so that the signature of the event can be better characterized.

B. Specimen Geometry/Preparation.

It has been demonstrated by other investigators that acoustic emission counts per unit time is a function of the volume of deforming material. As the volume decreases, the count rate also decreases. Reducing the specimen volume then, in concert with limiting the potential sources of acoustic emission, will accomplish the goal of spreading out the events and minimizing signal overlap to allow a proper characterization of the signals.

To this end, a micro-tensile specimen with button-head grip ends was chosen. The sample geometry is shown in Figure 1. The specimen is composed of the button-heads, a gage section and a sub-gage section. During tensile loading, plastic deformation was limited to the sub-gage region. From the specimen dimensions, it can be seen that this comprises a volume of material of about three cubic millimeters. In addition to minimizing the count rate, this also served to identify the location of the events and aid subsequent metallographic and fractographic analysis of the failed specimens.

The button-head configuration was chosen to minimize the number of signals possibly due to mechanical interference caused by misalignments of tensile loading and specimen axis. In the case of ideal alignment, the top and bottom grip centerlines are precisely in line with one another and with the centerline of the other components of the load train. Moreover, they are precisely in line with the specimen centerline. Departures from the ideal situation are caused by poor alignment of the top and bottom grip centerlines and inaccurate machining of the test specimen itself. A combination of these sources of misalignment always operate in any tensile test.[21] From an acoustic emission viewpoint, misalignment could significantly influence test results especially at low strains because it affects the average stress at which the transition from elastic to nonelastic deformation occurs and may introduce spurious sources of mechanical noise associated with the specimen and grip centerlines being forced into alignment during loading.

The button-head configuration chosen minimized misalignment by giving the specimen two-degrees of freedom by virtue of the square-shouldered bearing surface. Alignment of the specimen and loading axis for the third-degree of freedom was controlled by precise machining of the specimen shoulders to be flat and parallel. Additionally, the square-shouldered button-head was preferable to either tapered or spherical buttons because it minimized the contact area between the specimen and grips. The square shoulders eliminated the possibility of slippage between grips and specimen which could be present with the other shape ends and be a source of noise. Also, the inherently smaller contact area of the square-shoulder lessened the likelihood that spurious signals would be generated in the load system and detected as an acoustic emission event. Figures 2 and 3 show a specimen inserted into the grips.

---

[21] *B. W. Christ, S. R. Swanson, J. of Test and Eval., Vol. 4, No. 6, p. 405, 1976.*

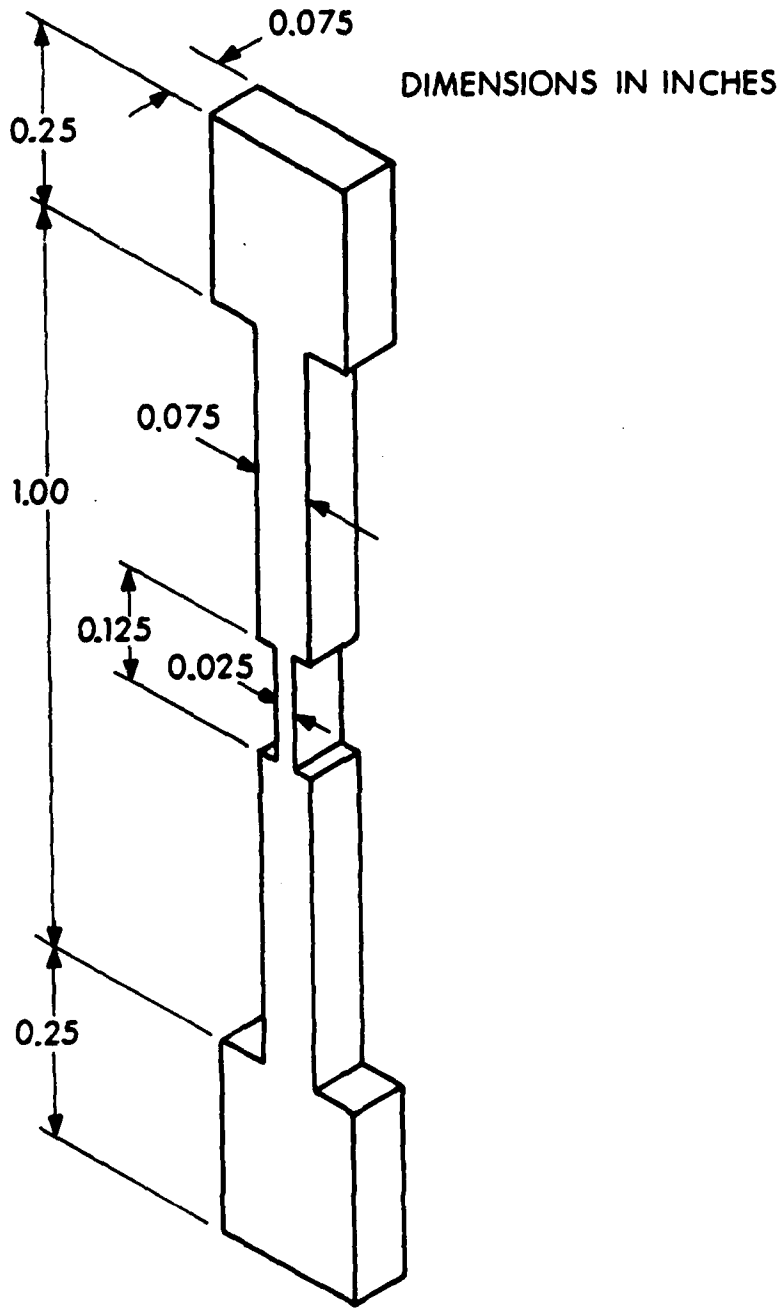

Figure 1. Dimensional Drawing of the Microtensile Specimen

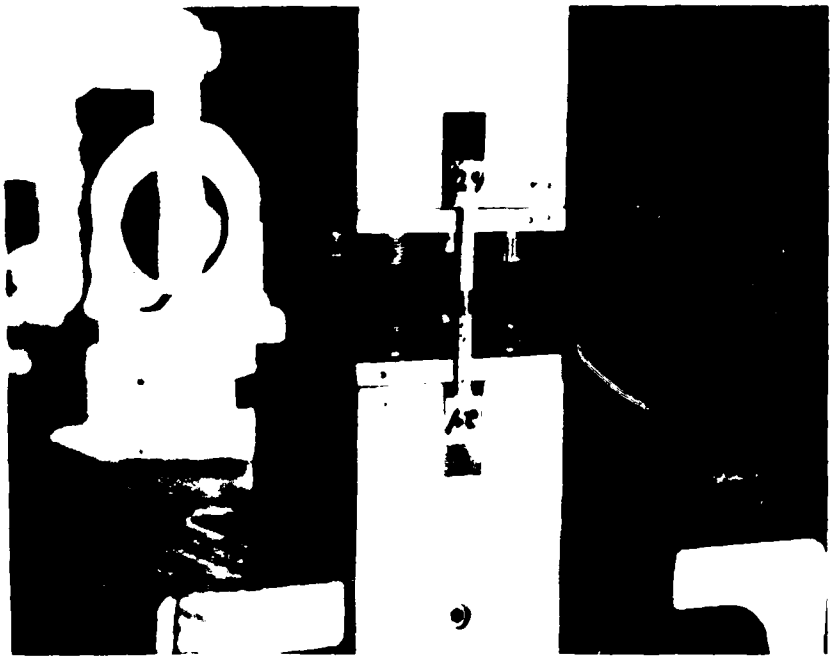

Figure 2. Microtensile Specimen Partially Inserted into Grips (Viewed from Side Opposite Optical Probe)

Figure 3. Microtensile Specimen Fully Inserted into Grips (Viewed from Same Side as Optical Probe)

As previously mentioned, inaccurate machining of the test specimen itself can lead to misalignment problems and additional sources of noise. For this reason and because the specimens were extremely small, particular care was taken to ensure that dimensions were true and the specimen was symmetric about the centerline. One-quarter inch thick plates of 304L stainless steel in the as-received condition were used to fabricate the specimen. All specimens were cut with their axes parallel to the rolling direction of the plate. The sequence of operations followed, starting with the initial plate stock to finished microtensile specimen, is shown in Figures 4 through 6. The sequence was as follows:

1. Plates were cut into 1.5 x 6.0-inch pieces and milled on both sides to a final thickness of 0.20-inch with all faces flat and parallel.

2. The specimen plate was placed in the milling machine and the gage section cut in one side only.

3. The sub-gage section was then milled into the gage.

This completes the machining of one-half of the specimen plate.

4. A block of aluminum was milled such that one face of the block had the negative contour of the specimen plate. The specimen plate was then placed in contact with the block. (Figure 4.) This was done to provide support while milling the opposite side of the specimen to minimize bending and resultant work hardening in the sub-gage section and to insure that the specimens were symmetric after completion of the milling operation.

5. A milling saw was then used to slice specimens from the plate as required. A final specimen plate is shown in Figure 5 prior to specimen cut-off.

Optical probing to detect acoustic emission places additional requirements on specimen preparation over and above careful machining practices. At least one surface must be flat and highly polished. This added the following steps to the specimen preparation operations:

6. Each specimen was mounted in a room temperature setting epoxy (Epo-Kwick). Adjacent to each side of the specimen was placed a bearing plate to eliminate rounding of the specimen face due to any rocking motion during polishing or preferential removal of the epoxy during the grinding and polishing operations. A mounted specimen is shown in Figure 6.

7. Specimens were then given a fine metallographic polish.

8. The mounted polished specimens were then placed in a bath of DECAP which dissolved away the epoxy mount leaving a finished specimen.

C. Load Frame.

A number of load frames/load systems were either tried or considered. These included conventional and non-conventional screw or hydraulic machines where the control variable is cross-head displacement. These machines had the disadvantage that significant noise was generated by the mechanical gearing or

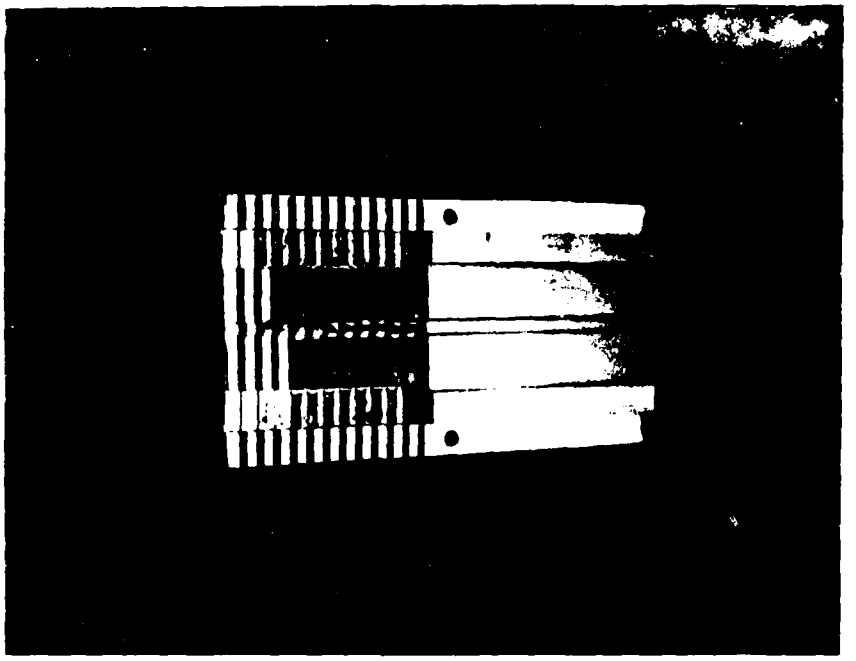

Figure 4. Microtensile Specimen Plate Shown Attached to Aluminum Milling Block

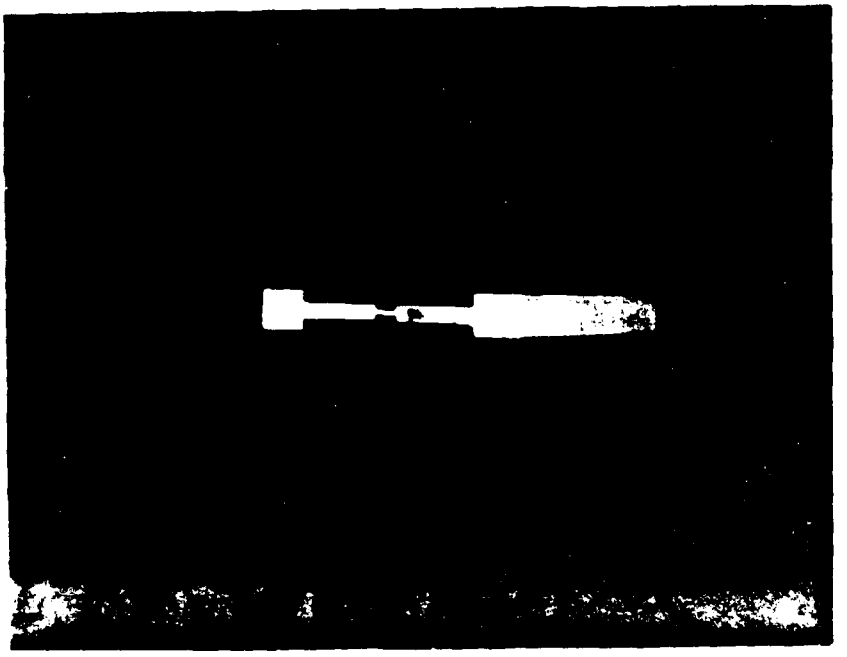

Figure 5. Finish Machined Microtensile Specimen Plate Prior to Specimen Cut-off

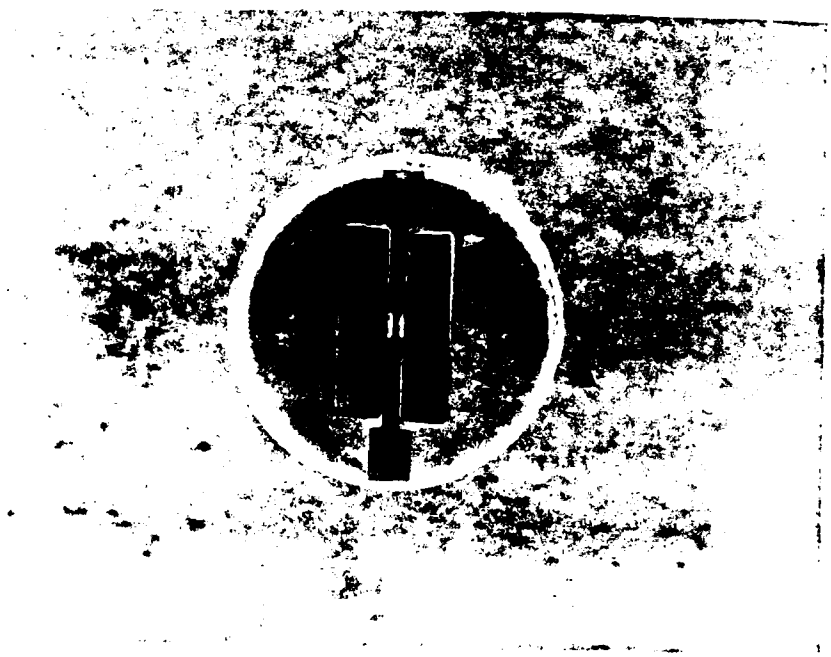

Figure 6. Microtensile Specimen Mounted for Final Polishing

the pumping of fluid through valves and orifices. These problems were overcome by using an Allied Research Associates pneumatic test machine modified to be compatible with testing of microtensile specimens and incorporating an optical interferometer. A general sketch of the basic load frame is shown in Figure 7. Load is applied by the action of pneumatic pressure on a pair of pistons. The operation of the system is analogous to the application of weights to a specimen: The control variable is load. That is, it is a dead-weight loading machine.

Figure 8 shows a cross-sectional schematic of the actuator cross-head. Piston-cylinder friction is kept to a minimum by the rolling piston seal. As can be seen, the pistons were not in contact with the cylinder walls, they were essentially free and self-centering in the cylinders. There was no metal-to-metal or sliding contact to act as a source of noise. The cylinders were pressurized using a 2500 psi tank of Argon gas regulated to yield a 50 psi maximum input pressure. This allowed for testing in the load range of 0-200 lbs., more than adequate for the microtensile specimens.

D. Optical Probe.

The use of an interferometer to detect acoustic emission was pioneered at The Johns Hopkins University. Early studies centered on the detection of acoustic emission in relatively large mass specimens undergoing primarily brittle type failure, e.g. stress-corrosion cracking in steel, thermal cracking in glass, etc. For the present effort a new interferometer was designed based on Fizeau optics to measure acoustic emission during tensile tests.[18] The intention was to produce a system less sensitive to room vibrations and atmospheric disturbances than the previously used Michelson designs. Additionally, the Michelson design was sensitive to torsional vibrations of the base plate and the Fizeau optics eliminated this problem. Figure 9 is a diagram of the improved Fizeau optical arrangement. An expanded laser beam is incident from the left and is focused by the lens on the specimen surface. Approximately half of the incident light is reflected by the beam splitter and focused on the reference mirror R. The two beams, one reflected from the specimen and one reflected from the reference mirror, are recombined at the beam splitter and produce a fringe pattern at the output which is focused on the photodetector.

Figure 10 shows details of the reference mirror drive. The mirror itself is mounted on a 1/8-inch diameter, 1/2-inch long piezoelectric tube and provides possible correction of vibrations with amplitude up to about 6 fringes, with a 1 msec response time. The PZT tube in turn is mounted on a spring steel strip which can be magnetically moved to provide a low frequency correction of about 6000 fringes. This large range of correction was designed to compensate for dimensional changes in the tensile specimen. A photograph of the mounted interferometer is shown in Figure 11. When actual testing was begun, it was found that correction electronics produced sufficient feedback noise that the signal recorder would be triggered. Consequently, it was necessary to run the tests without the correction electronics at all. To accomplish this, certain modifications had to be made to the load system to eliminate spurious vibrations. First, the load frame with the interferometer attached was placed on a rigid optical table. Between the load frame and table was placed a four-inch thick foam rubber pad two feet wide by four feet long. On this pad was

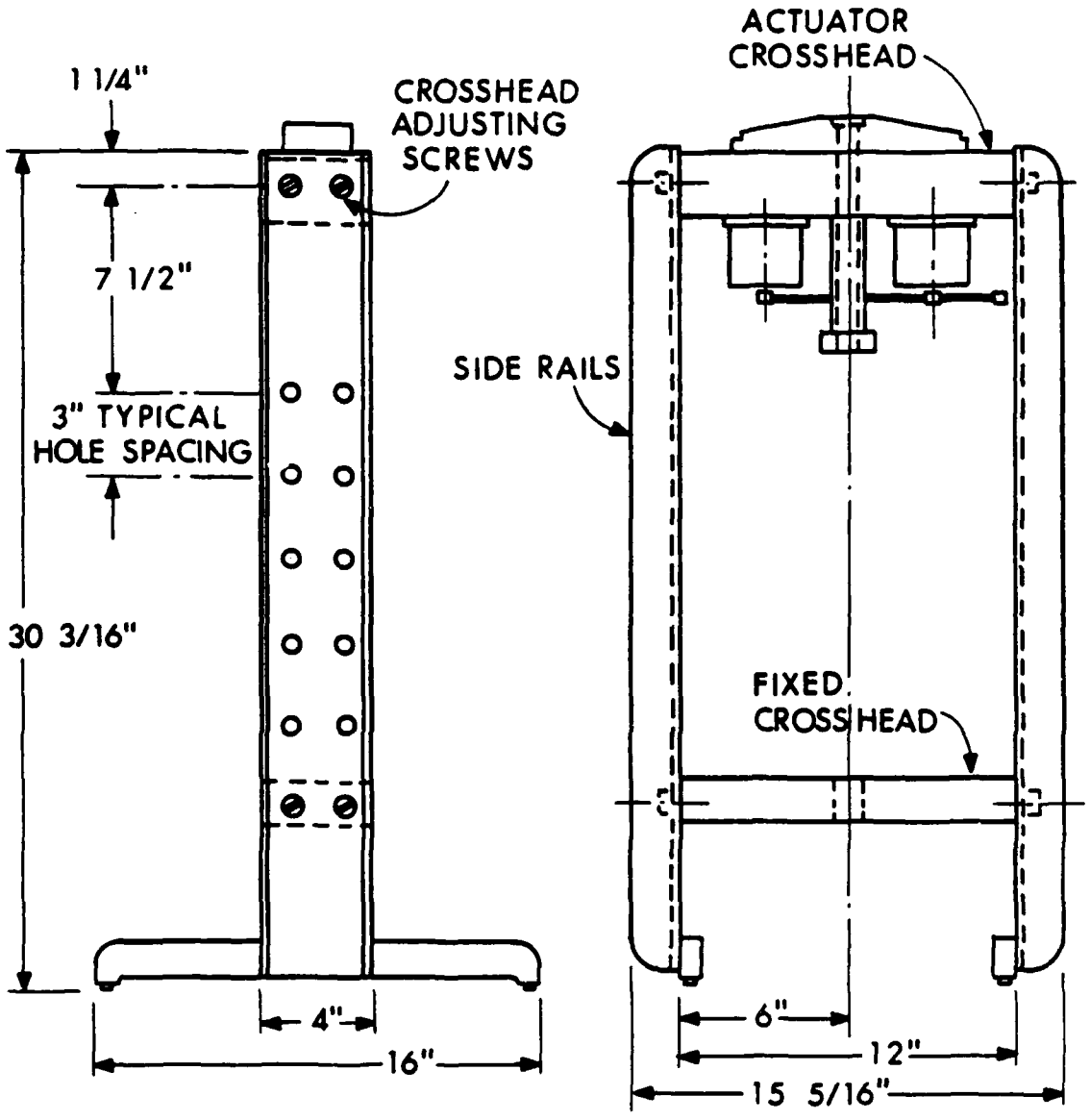

Figure 7. Drawing of Pneumatic Load Frame Used for Tensile Testing

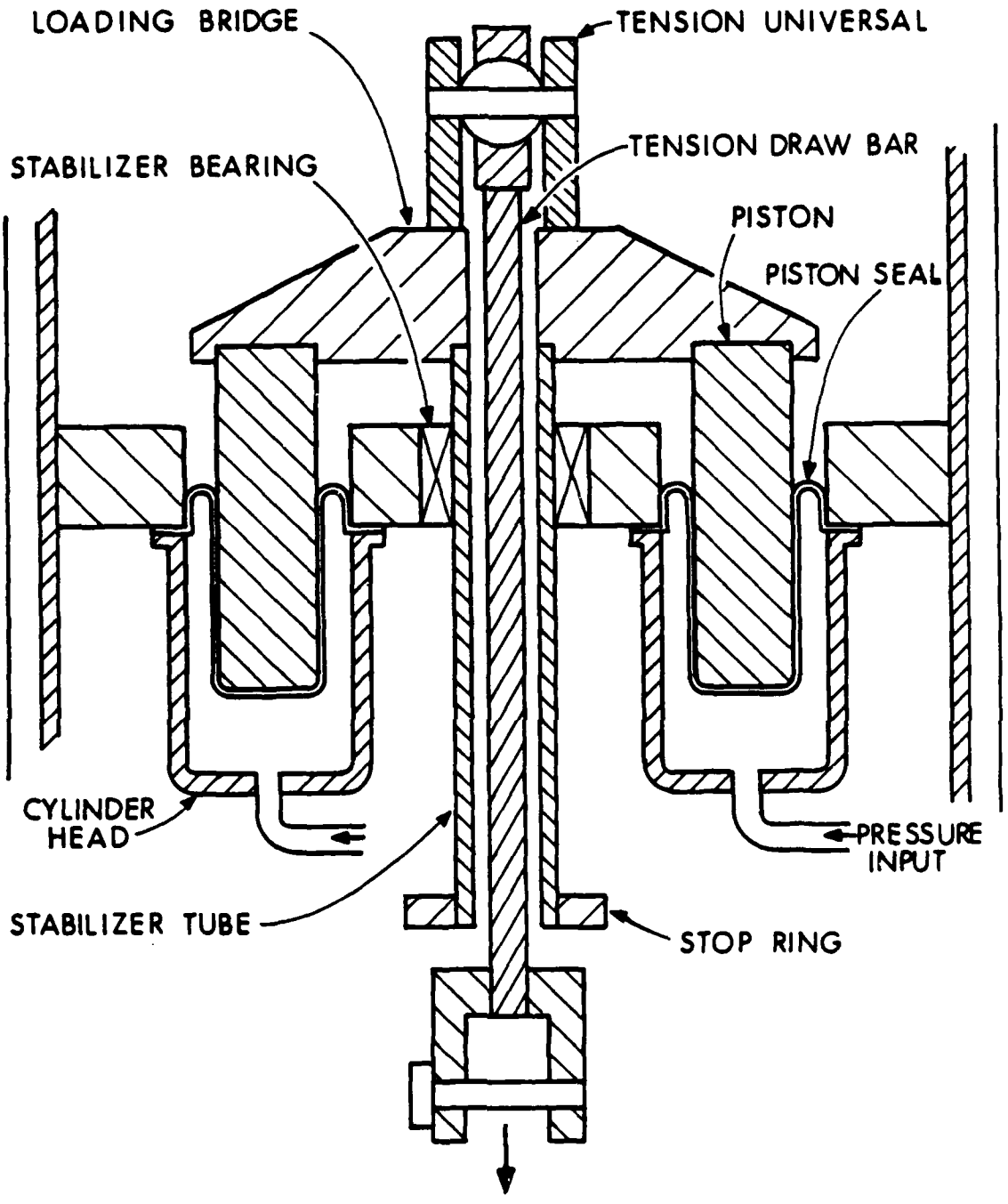

Figure 8. Detailed Drawing of Actuator Cross-head Showing Details of Rolling Piston Seal

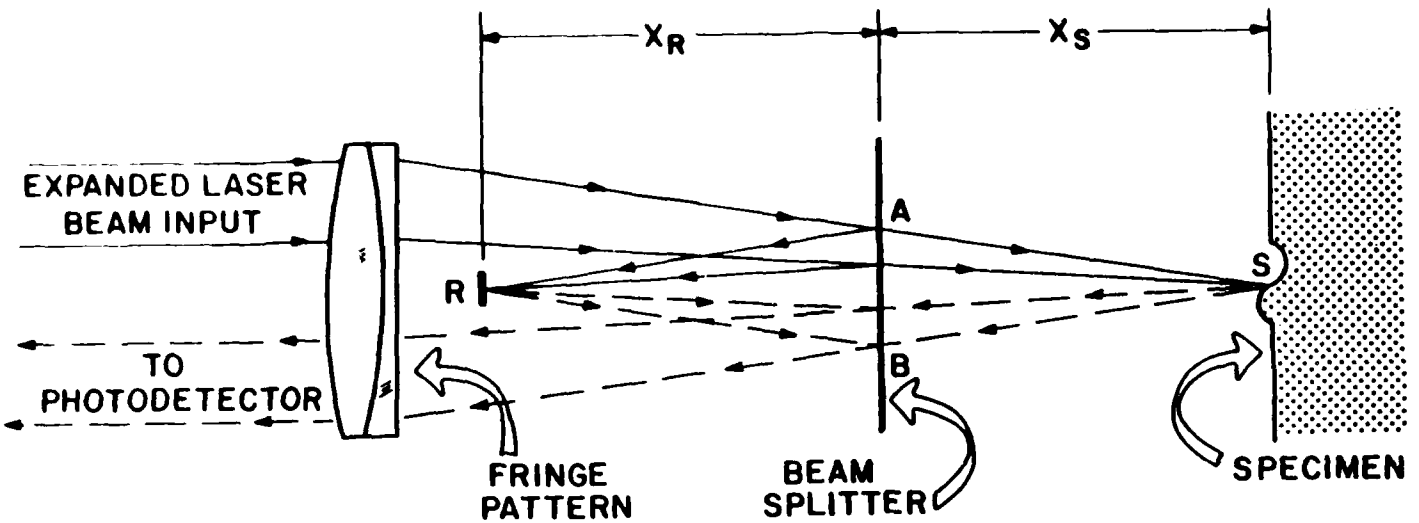

Figure 9. Optical Arrangement of Fizeau Interferometer Used to Study Acoustic Emission during Plastic Deformation

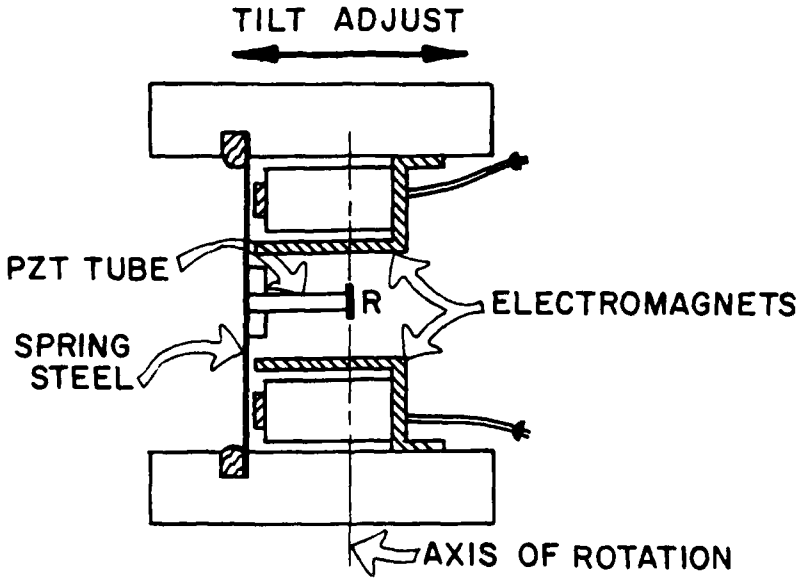

Figure 10. Details of Reference Mirror Drive Used to Isolate the Interferometer from Vibrations and Dimensional Changes of the Specimens

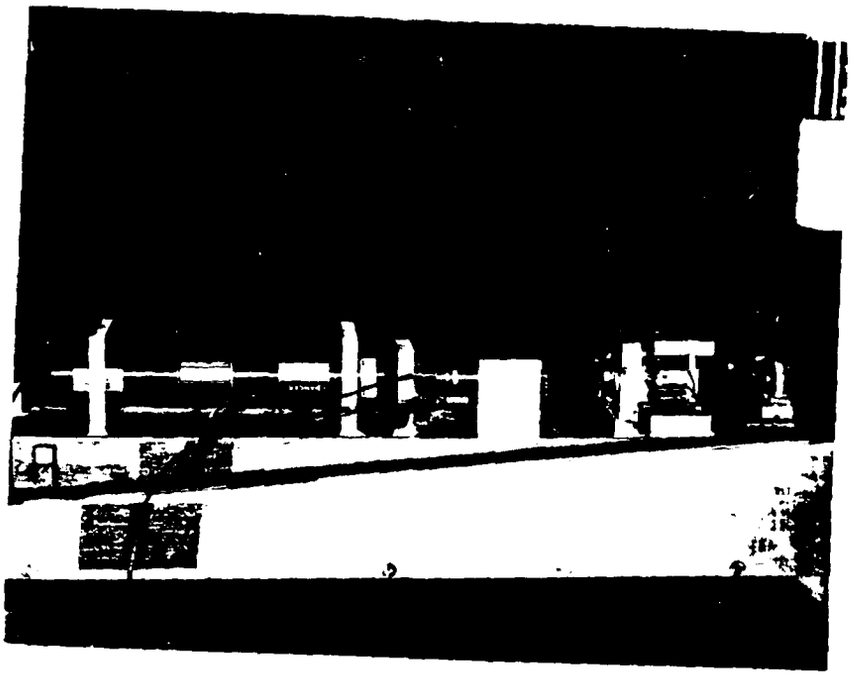

Figure 11. Fizeau Interferometer Mounted on Load Frame

Figure 12. Overall View of Load Frame and Instrumentation

placed a three-quarter-inch thick sheet of plywood. The load frame was then placed on the plywood. The entire arrangement can be seen in Figure 12.

The second, and perhaps most important, modification was the elimination of any flexural vibrations that could be picked up along the tensile axis. This was accomplished by attaching a piston between the load cell and the tensile drawbar and attaching a thick-walled polyethylene cylinder to the actuator cross-head. As a load was applied to the specimen, this tightly fitting piston was drawn through the polyethylene cylinder (or stabilizer). The piston and cylinder were hand-honed and lubricated to provide a smooth sliding contact.

When these modifications were completed, it was found that the interferometer was extremely stable. Random fringe motion due to room vibrations and atmospheric disturbances was not more than about 0.1 fringe under normal conditions.

E. Event Recording and Waveform Analysis.

Output from the optical probe photodetecter was fed into a 20 db amplifier and from these into a Nicolet Explorer Digital Oscilloscope. When a sweep trigger signal (an acoustic emission event) is received, the scope's analog-to-digital convertor measures the signal at intervals and transfers the information to its buffer memory. Full-scale voltage was set at 200 mv and the sampling interval was 50 nsec per point. On each trigger signal, 4096 points were captured. This provided a signal window of approximately 0.2 milliseconds. On completion of each sweep, the waveforms were transferred to a magnetic disk memory for later analysis.

The data stored in the magnetic disk memory was transferred at a later time to a Hewlett-Packard 9845A computer for waveform analysis. Computer programs were written to produce graphic output of the captured signals and Fast Fourier transform analysis of the time domain data. The option of analyzing either the whole waveform or only selected regions of interest was also available. The scope sampling rate permitted the identification of signal frequencies as high as 10 MHz. Since this top frequency is higher than that seen in previous spectrum analysis studies, particular care was taken to be sure that any signal components received in the upper frequency realm were not an artifact of the optical probe, digital oscilloscope or Fast Fourier transform analysis. Various calibrated test signals (since waves and saw-tooth ramp functions) were fed into the system over the full frequency range. In all cases, the resultant Fast Fourier transform produced the expected frequency spectrum, centered on the signal frequency with very minimal off-frequency components. It was concluded that for the actual waveforms captured during the tensile loading experiments the waveform analysis would truly indicate the frequencies present in the range of 0-10 MHz.

III. RESULTS

Microtensile specimens were tested in the pneumatic loading machine until failure. The rate of loading was adjusted such that specimen failure occurred within approximately 10-20 minutes. During each test, load versus time was recorded continuously until failure. Restrictions due to constraints

imposed by specimen size and equipment configuration prevented simultaneous recording of displacement or strain. A series of independent tests was run using an Instron screw-type test machine. No acoustic emission measurements were attempted during these tests. Their purpose was to obtain an approximate engineering stress vs. engineering strain curve for comparison with published engineering data to determine if the specimens were small enough to result in anomalous behavior. An average stress-strain curve is shown in Figure 13. Values obtained from standard engineering handbooks were in general agreement with this data. This data demonstrated that while the gage section of the microtensile specimen was extremely small compared to standard engineering test specimens, it was still relatively large on a microstructural scale and thus it can be inferred that the acoustic emission data gathered during the dead weight loading tests should be representative of the bulk material.

A. Surface Examination.

Prior to, during, and after each acoustic emission test, each specimen was examined optically. Figure 14 shows the undeformed unetched surface of a test specimen. Both optical and SEM examinations of the surface failed to reveal any unusual features such as prior slip, twinning, or broken intermetallic particles which could possibly confuse subsequent correlation with the acoustic emission events. During subsequent loading, the specimen subgage section was observed under low power magnification. During the load cycle, the subgage lost its polished appearance and became frosted. This was the reason the optical probe was focused on a spot immediately adjacent to the deforming area. During the later stages of loading, the reflected beam would have become weak or have been deflected from the photodetector. Just prior to failure, a close examination revealed that the specimen subgage had a "Swiss cheese" appearance. Being a very ductile material, the 304L stainless steel failed due to void nucleation, growth and coalescence. During the final stage of deformation, void coalescence and failure of the remaining ligaments was observed. In each of the tests failure occurred at the mid-plane of the subgage section.

In addition to the above observation at failure, specimens were removed from the test fixture just prior to failure. Figure 15 shows an SEM picture of one such specimen. Note the necking of the subgage at its mid-plane. None of the observations revealed any evidence of cracks located on the surface. Failure was due to void coalescence.

The surface of each specimen was examined optically after failure. Figure 16 shows the area near the shoulder of the subgage section. Extensive formation of slip bands can be seen in nearly all the austenite grains. The number of slip bands is in the thousands when summed over the whole subgage area. Figure 17 is an SEM picture of the slip bands formed in a single austenite grain. Figure 18 is an optical photograph closer to the mid-plane of the gage section. Severe deformation and limited depth of field of the optical microscope made focusing difficult. However, it can still be clearly seen that the individual austenite grains have been moved significantly from their original positions. The beginnings of grain pullout can be seen with a corresponding contraction of the material between the grains. The surface grains in the gage section number in the hundreds.

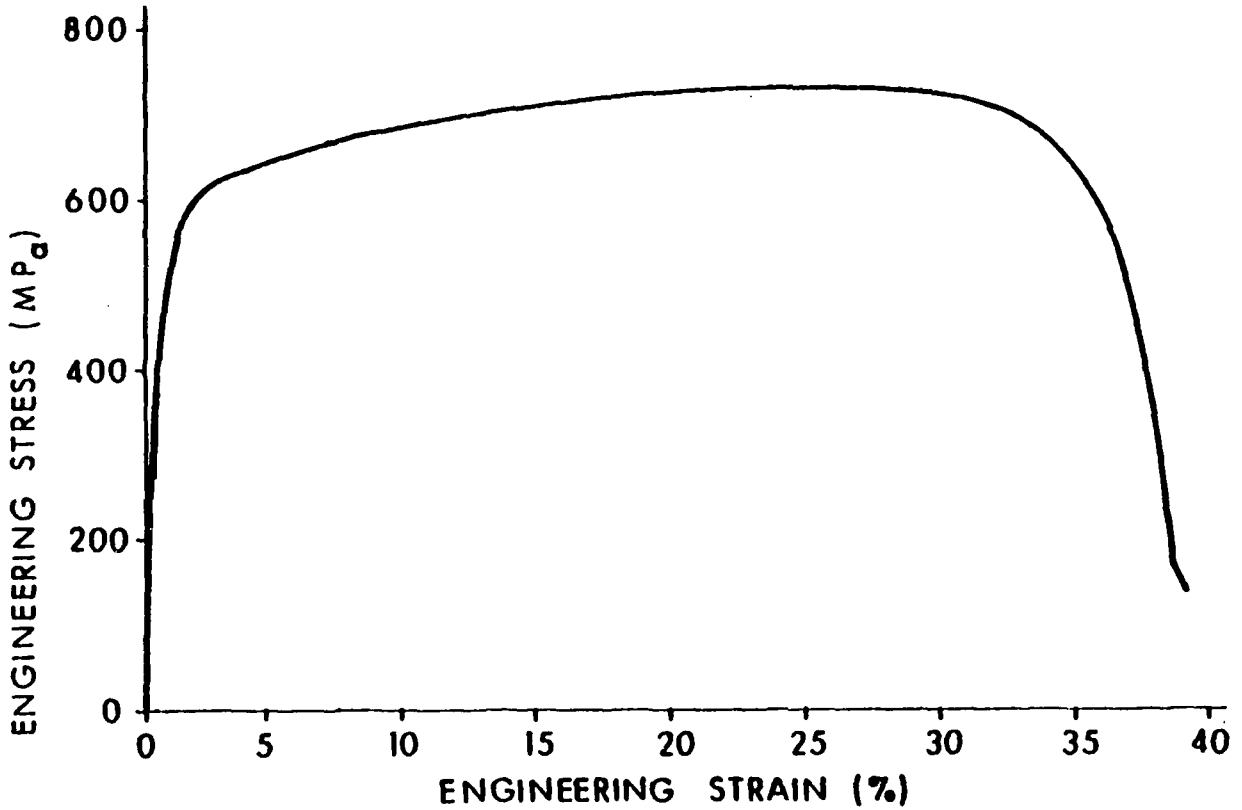

Figure 13. Nominal Stress-strain Curve for 304L Stainless Steel Microtensile Specimens

Figure 14. Surface of Specimen Prior to Tensile Loading (100X)

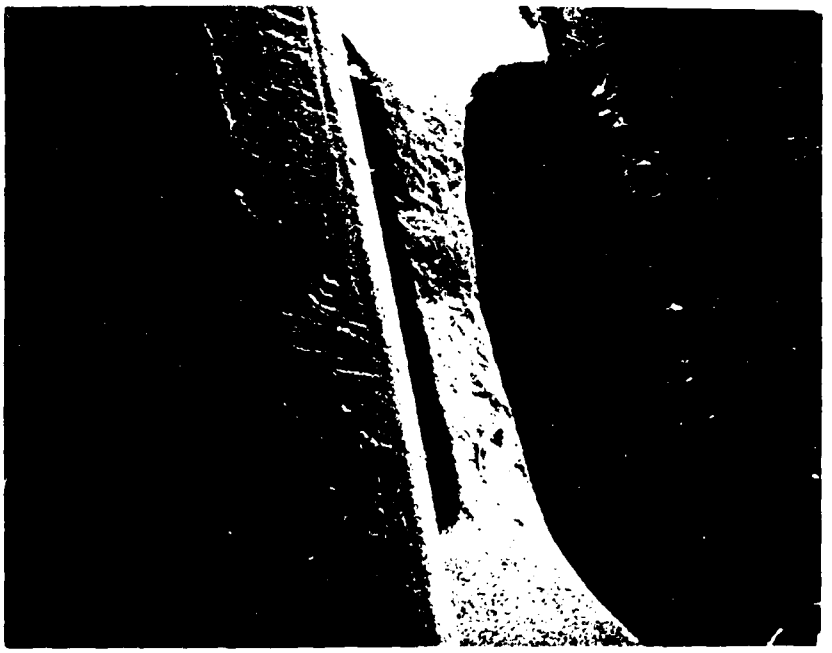

Figure 15. SEM Photograph of Test Specimen Just Prior to Failure. (Area shown is the subgage section) (70X)

Figure 16. Optical Photograph of Subgage Region of the Specimen After Failure (100X)

Figure 17. SEM Photograph of Slip Bands Formed During Tensile Loading (500X)

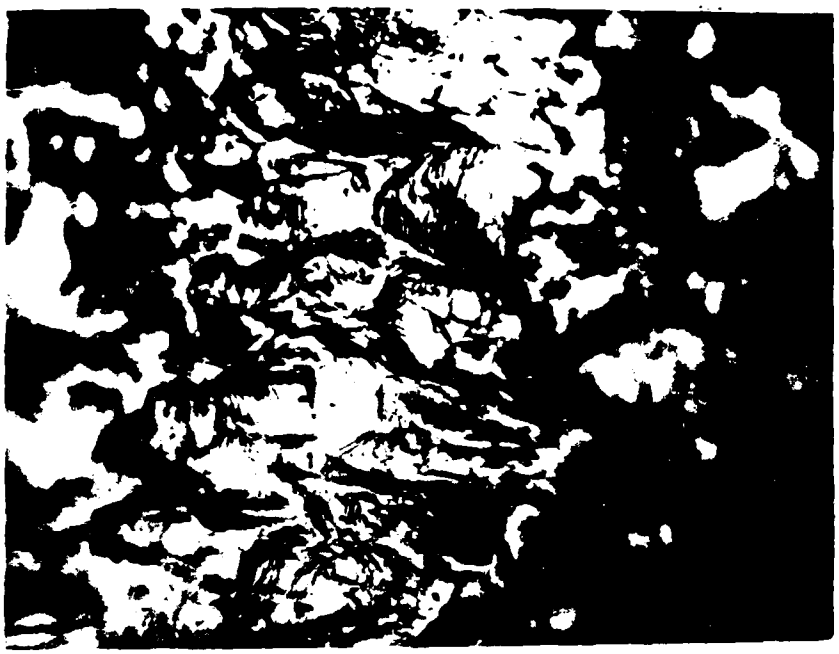

Figure 18. Optical Photograph of Deformed Subgage Region Showing Grain Motion (200X)

Figure 19. SEM Photograph of Fracture Surface of Test Specimen (70X)

B. Fracture Surface Examination.

The fracture surface of each failed specimen was examined in an SEM. Figure 19 shows the fracture surface of one such specimen at 70X. Even at this low magnification one can see many relatively large voids on the fracture surface. At slightly higher magnification (500X), it can be seen that each of these voids contains a rather large intermetallic particle (Figure 20). Figure 21 is a high magnification photograph of one such particle. At the base of some of these voids were particles that had failed in a brittle manner (Figures 22 and 23). The surface was scanned and a count made of the number of these broken intermetallics for later correlation with the acoustic emission signals. Not all the particles were intact or fractured. Some, as seen in Figure 24, were only partially failed.

C. Acoustic Emission Waveforms.

On the average, 100-150 waveforms were captured during the load cycle of each specimen. Invariably the signals fell into two categories. The first, designated a Type I waveform, had a rise time of approximately 0.25μs and a duration of 0.50μs. Figures 25, 28, 31 and 34 show four such waveforms. The similarity between the waveforms is striking. In each, the signal is characterized by a single high amplitude peak. Figures 26, 29, 32 and 35 show the frequency spectra of each of the waveforms from 0-10 MHz. Figures 27, 30, 33 and 36 show expanded frequency spectra from 0-2.5 MHz. It can be seen that each of the waveforms has two strong characteristic frequencies present. One located at 100 kHz and the other at 225 kHz. These signals are indeed representative of the hundreds of nearly identical Type I waveforms captured; the data suggests two things. First, the micro-tensile specimens in concert with the optical probe permit the recording of the signals with as little microstructural distortion as possible. Secondly, the near identical waveforms and frequency spectra suggest that a single mechanism is the cause of these signals.

The second waveform, designated Type II, is shown in Figures 37 through 64. As stated in the description of the digital oscilloscope used, when a sweep trigger signal was received 4096 data points sampled at a rate of 50 ns per point were stored. Consequently, each captured waveform had a duration of 0.2 milliseconds and could contain more than one event. This is evident when viewing the waveforms. Also shown in the figures, are some of the individual events extracted from the waveform. Comparison with the Type I event waveform show the Type II event to be greater than the Type I in amplitude. Whether one examines the frequency spectrum of the full waveform or the frequency spectrum of an individual event, two things are apparent. First, there are high frequency components of the Type I waveform appearing at approximately 7.5 MHz and 8.5 MHz. Secondly, the predominant frequencies of the Type I event are still present in the kilohertz regime. This suggests that the Type II event is caused by a mechanism which also triggers the occurrence of the Type I event.

The appearance of the high frequency components in the signal again reflect the advantages of the micro-tensile specimen and optical probe. The broad flat frequency response (0-10 MHz) of the optical probe permit faithful recording of signals on the 7.5-8.5 MHz region as stated earlier, high frequency components of a signal will be strongly attenuated in a material. Even with the optical probe near the deforming surface of a standard size

Figure 20. SEM Photograph of Fracture Surface of Test Specimen Showing Voids and Intermetallic Particles (500X)

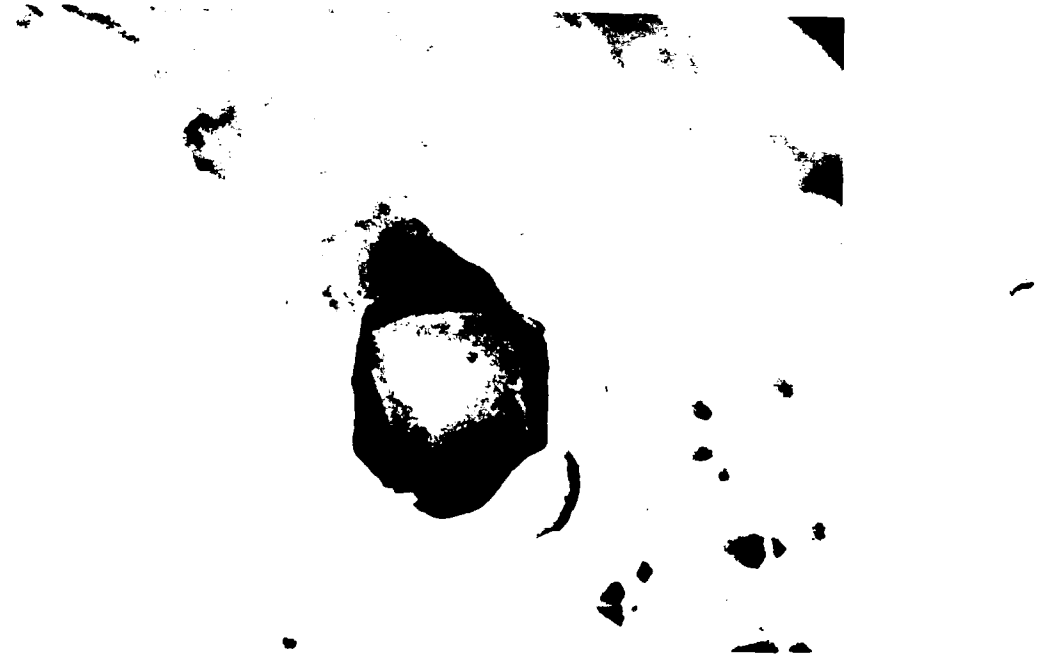

Figure 21. SEM Photograph of a Particle at the Bottom of a Void Located on the Specimen Fracture Surface (2000X)

Figure 22. Typical SEM Photograph of a Fractured Particle (2100X)

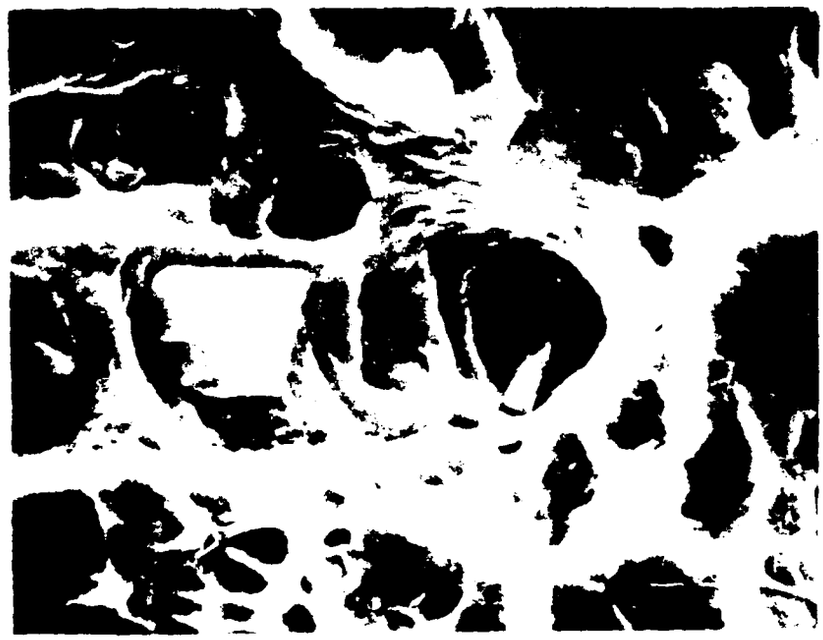

Figure 23. Typical SEM Photograph of a Fractured Particle (4500X)

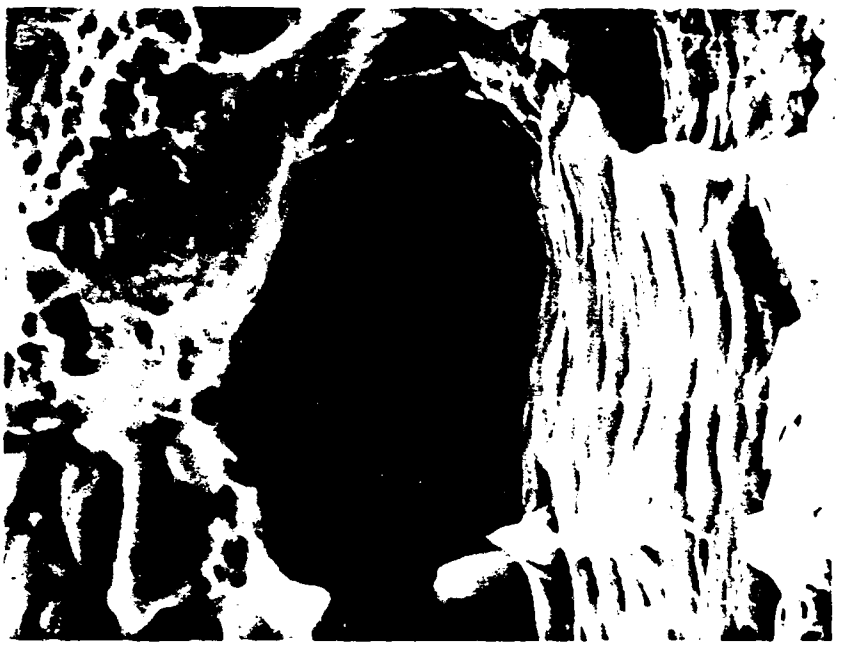

Figure 24. SEM Photograph of Partially Failed Particle (4500X)

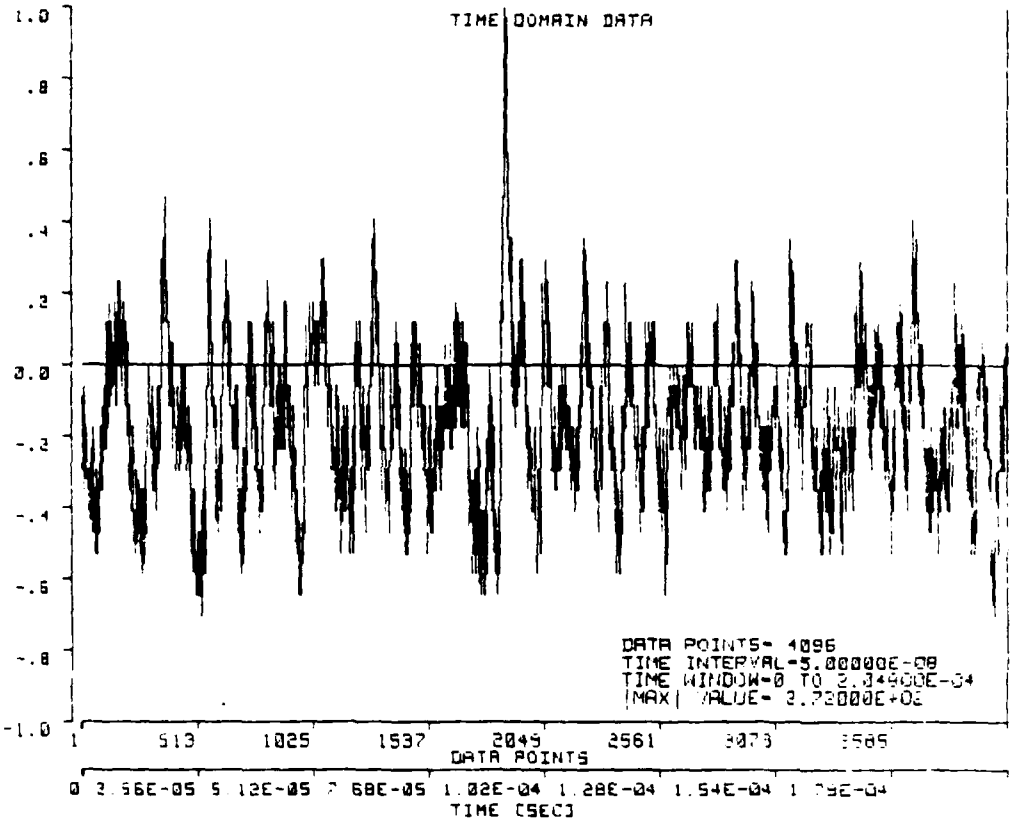

Figure 25. Typical Type I Waveform Observed during Deformation of a 304L SS Microtensile Specimen

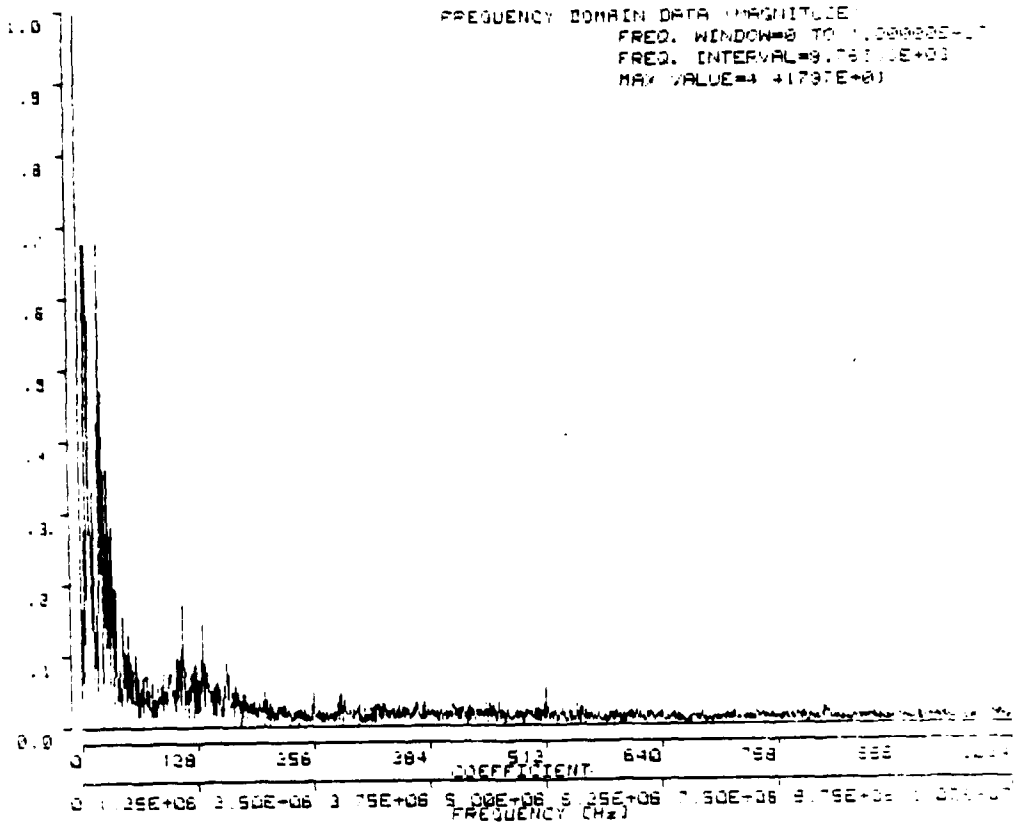

Figure 26. Frequency Spectrum of the Type I Waveform Shown in Figure 25, for 304L SS

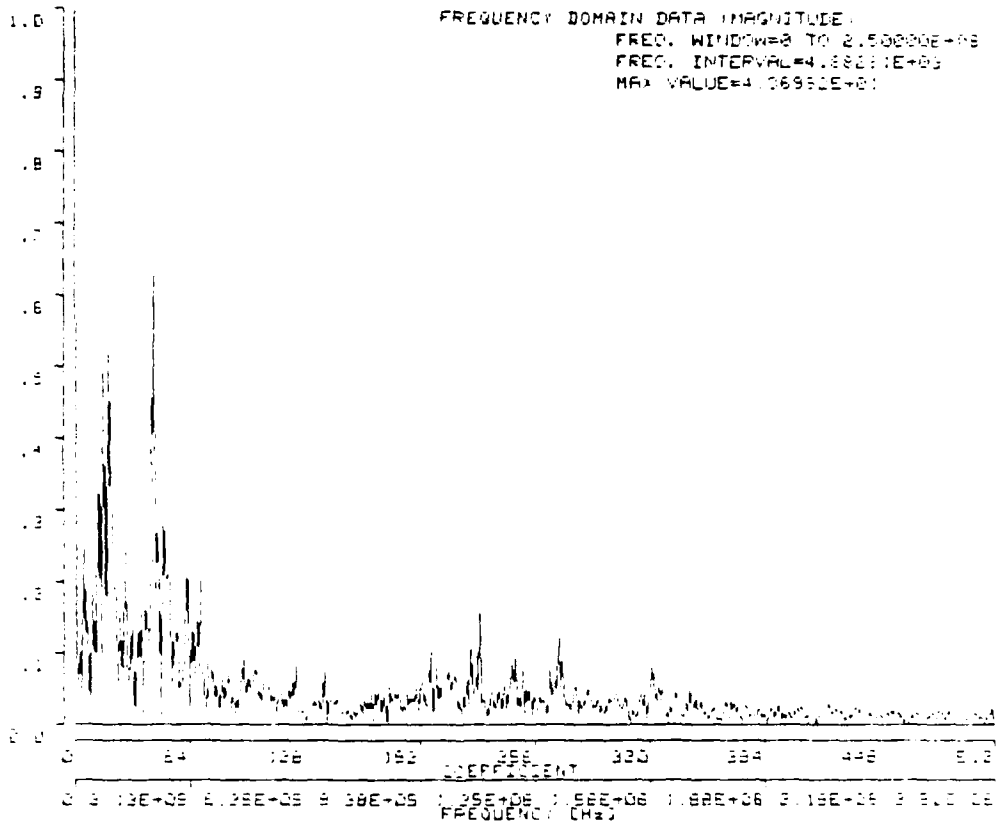

Figure 27. Expanded Frequency Spectrum of the Waveform Shown in Figure 25, for 304L SS

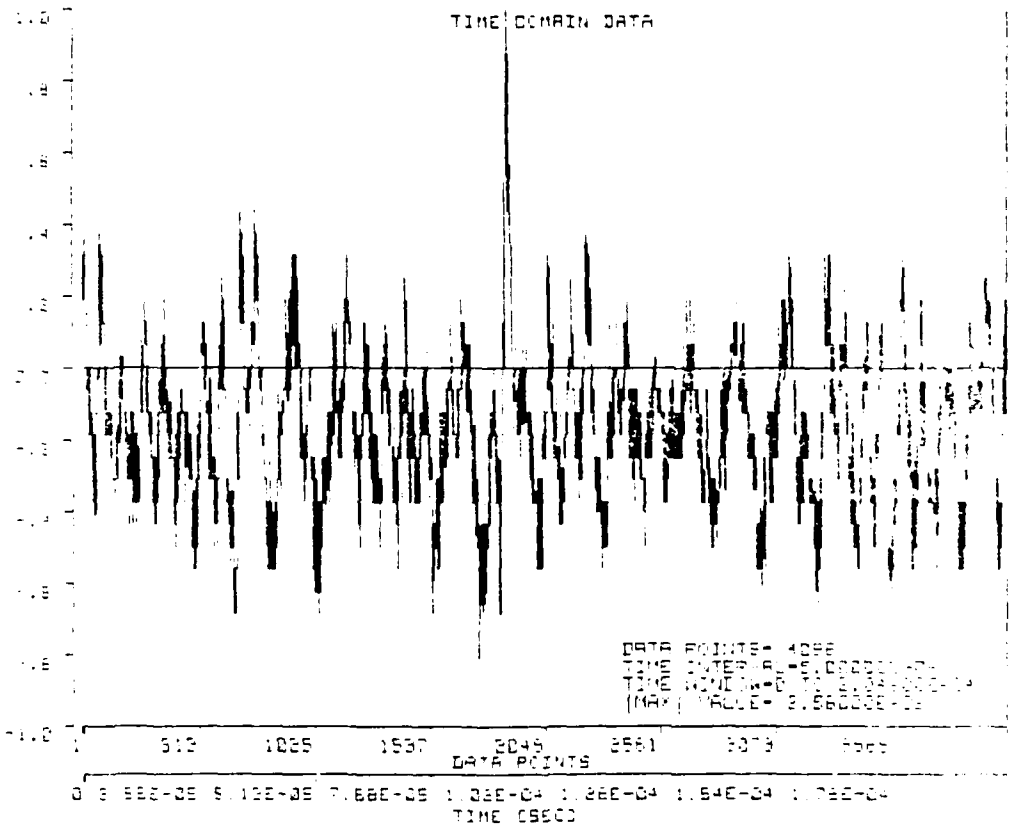

Figure 28. Typical Type I Waveform Observed During Deformation of a 304L SS Microtensile Specimen

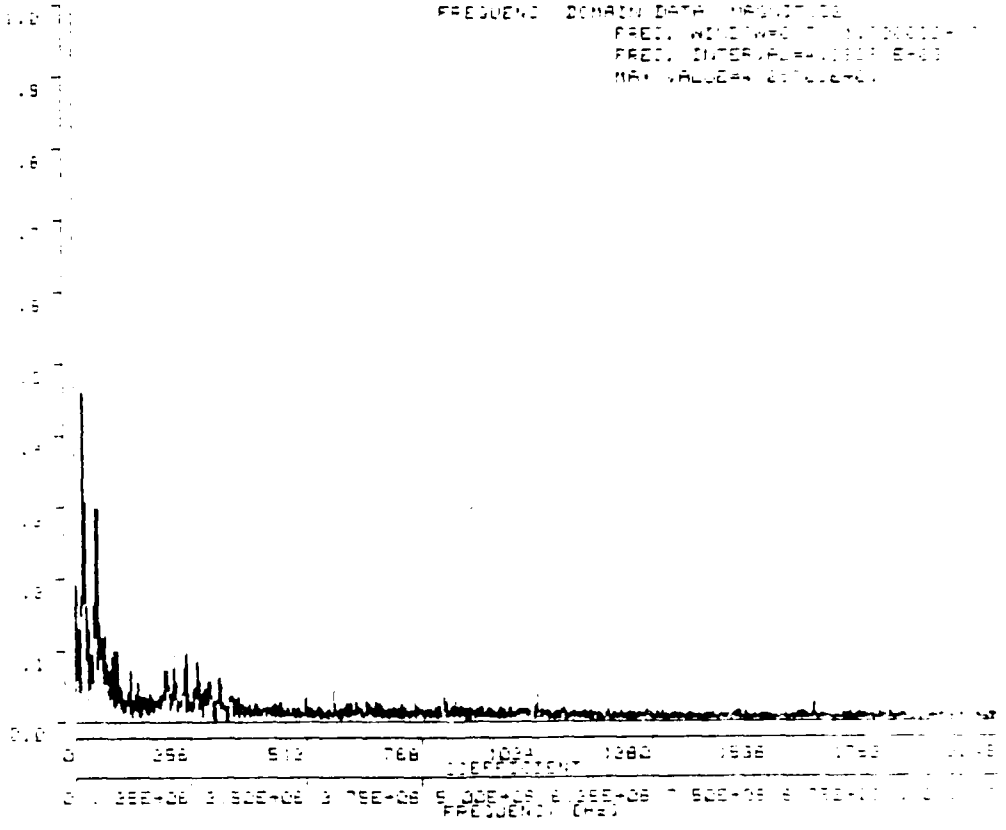

Figure 29. Frequency Spectrum of the Type I Waveform Shown in Figure 28, for 304L SS

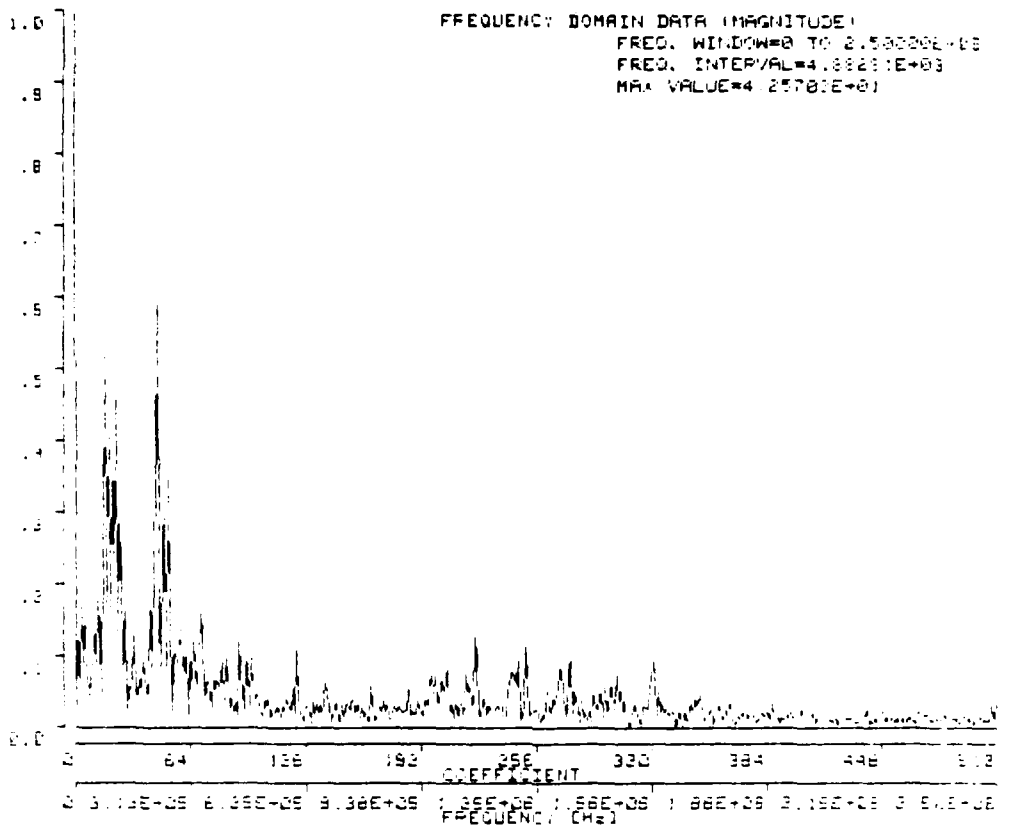

Figure 30. Expanded Frequency Spectrum of the Waveform shown in Figure 28, for 304L SS

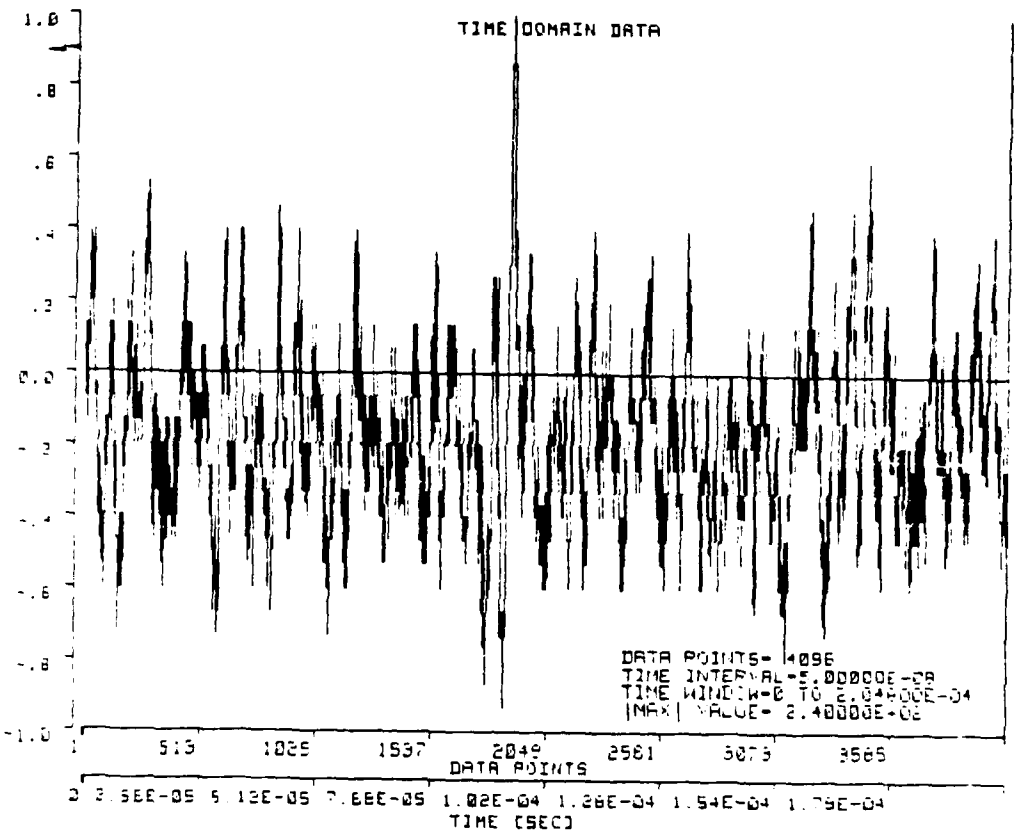

Figure 31. Typical Type I Waveform Observed During Deformation of a 304L SS Microtensile Specimen

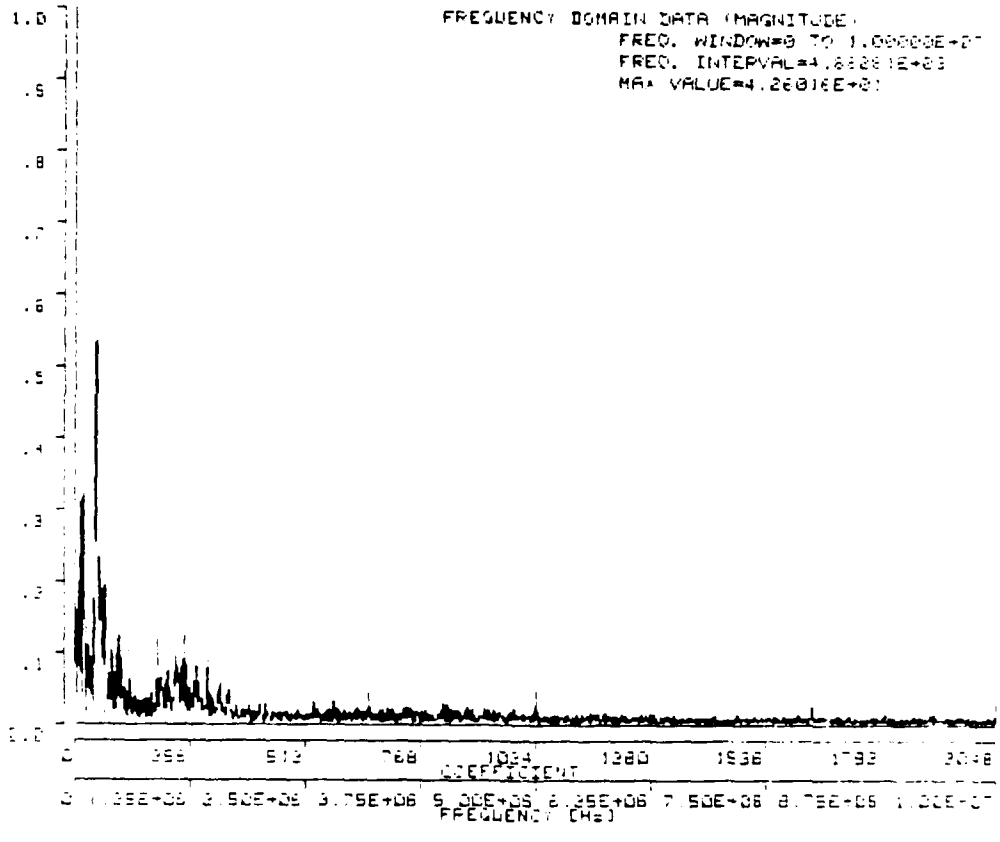

Figure 32. Frequency Spectrum of the Type I Waveform Shown in Figure 31, for 304L SS

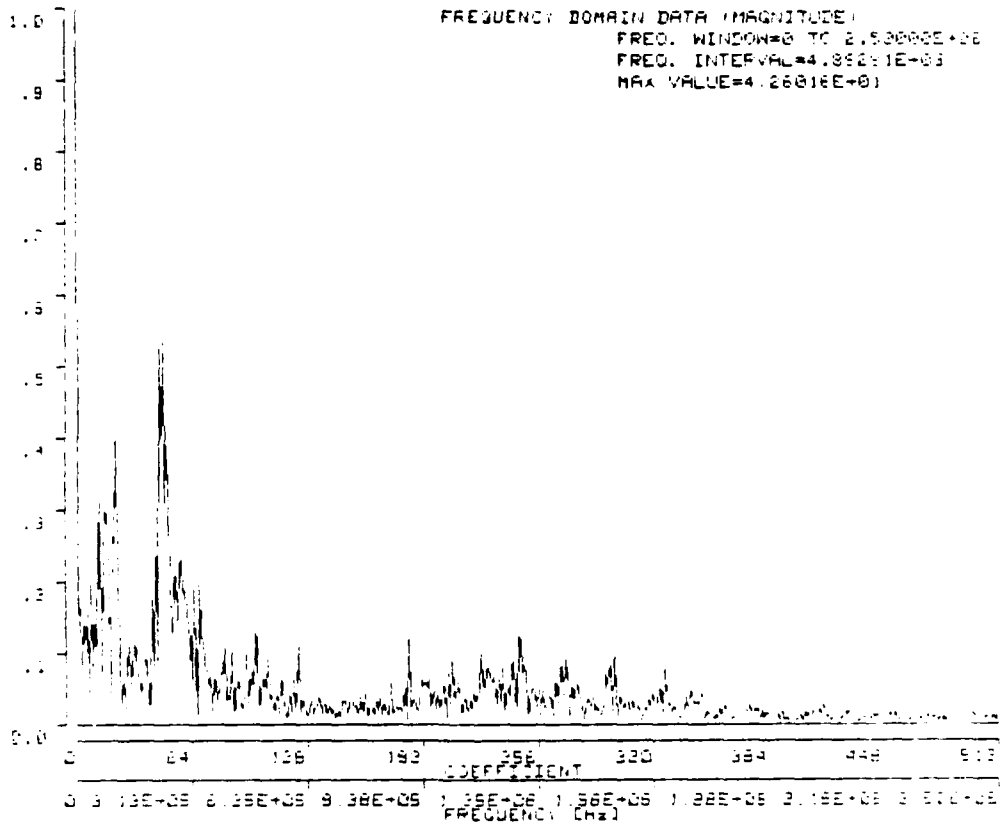

Figure 33. Expanded Frequency Spectrum of the Waveform Shown in Figure 31, for 304L SS

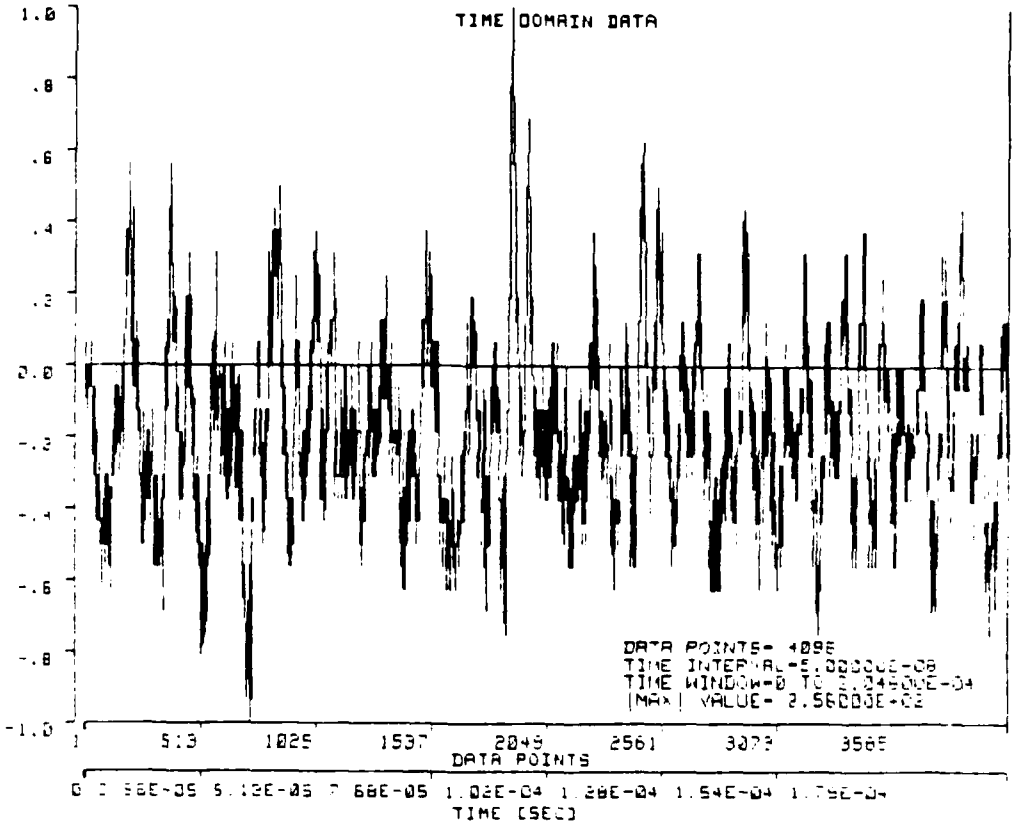

Figure 34. Typical Type I Waveform Observed During Deformation of a 304L SS Microtensile Specimen

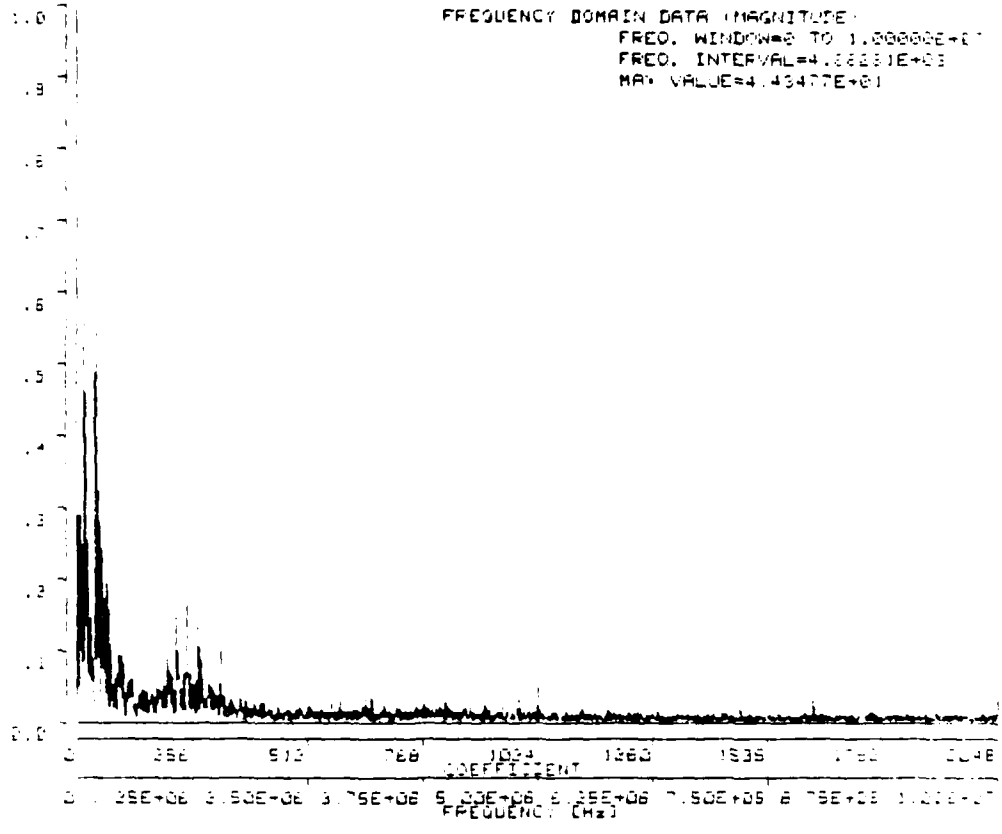

Figure 35. Frequency Spectrum of the Type I Waveform Shown in Figure 34, for 304L SS

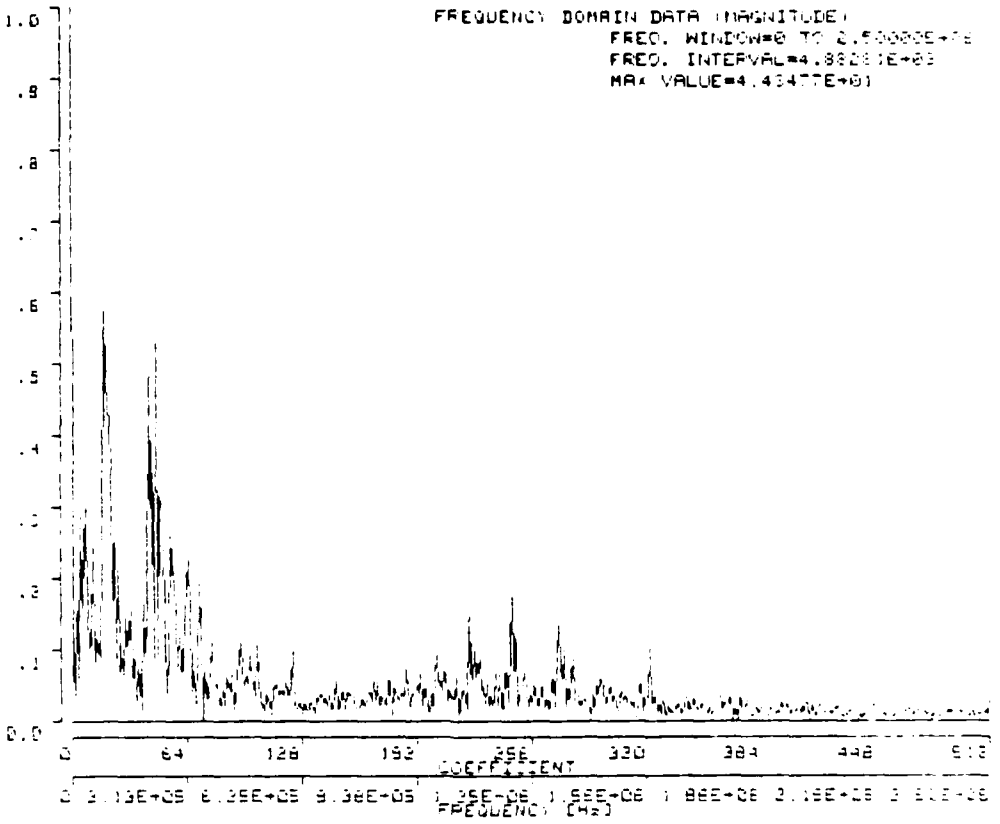

Figure 36. Expanded Frequency Spectrum of the Waveform Shown in Figure 34, for 304L SS

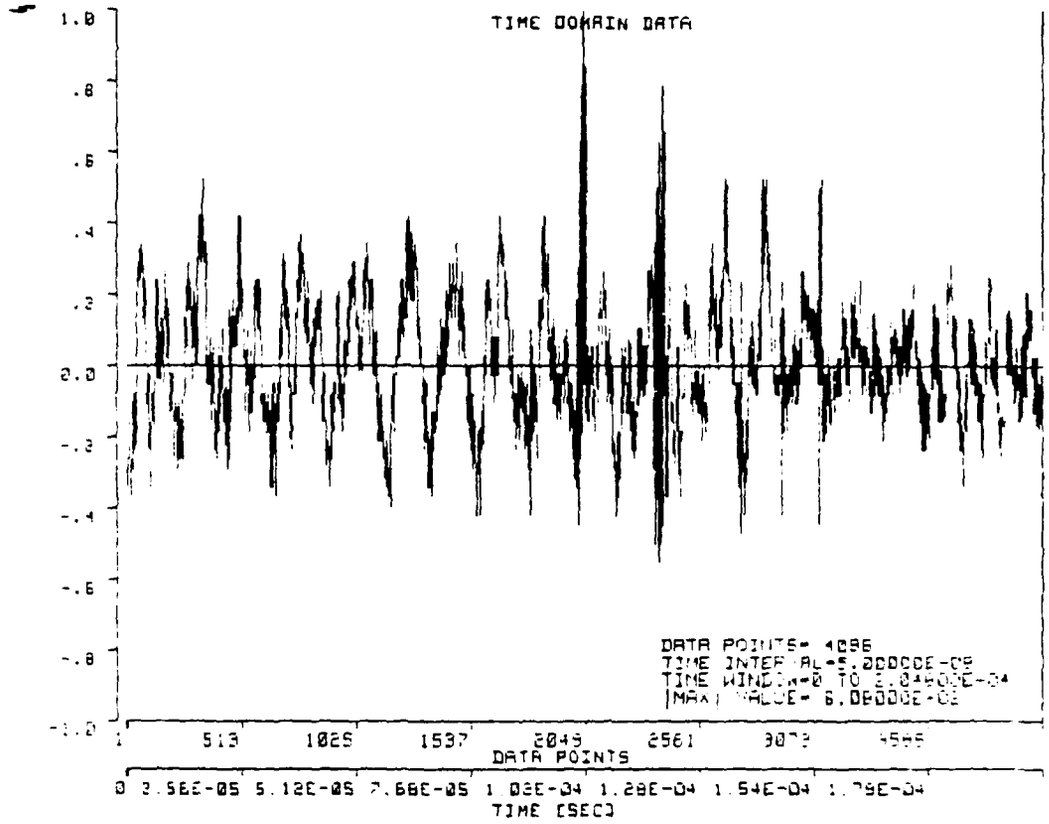

Figure 37. Typical Type II Waveform Observed During Deformation of a 304L SS Microtensile Specimen

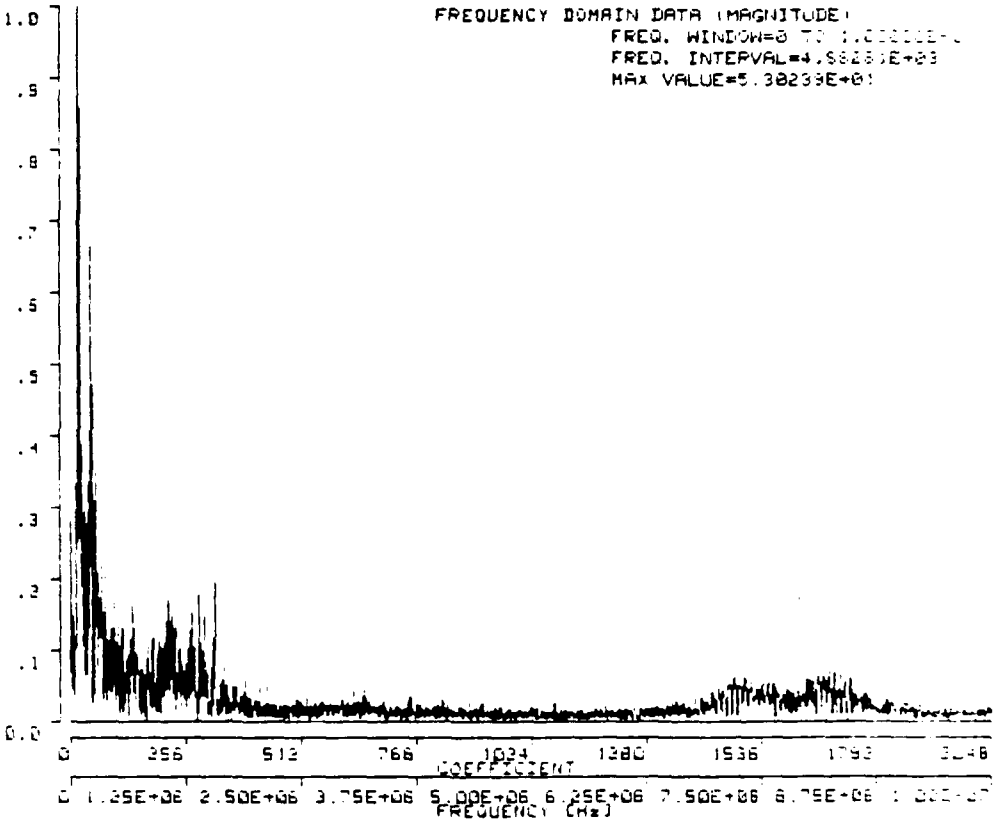

Figure 38. Frequency Spectrum of the Type II Waveform Shown in Figure 37, for 304L SS

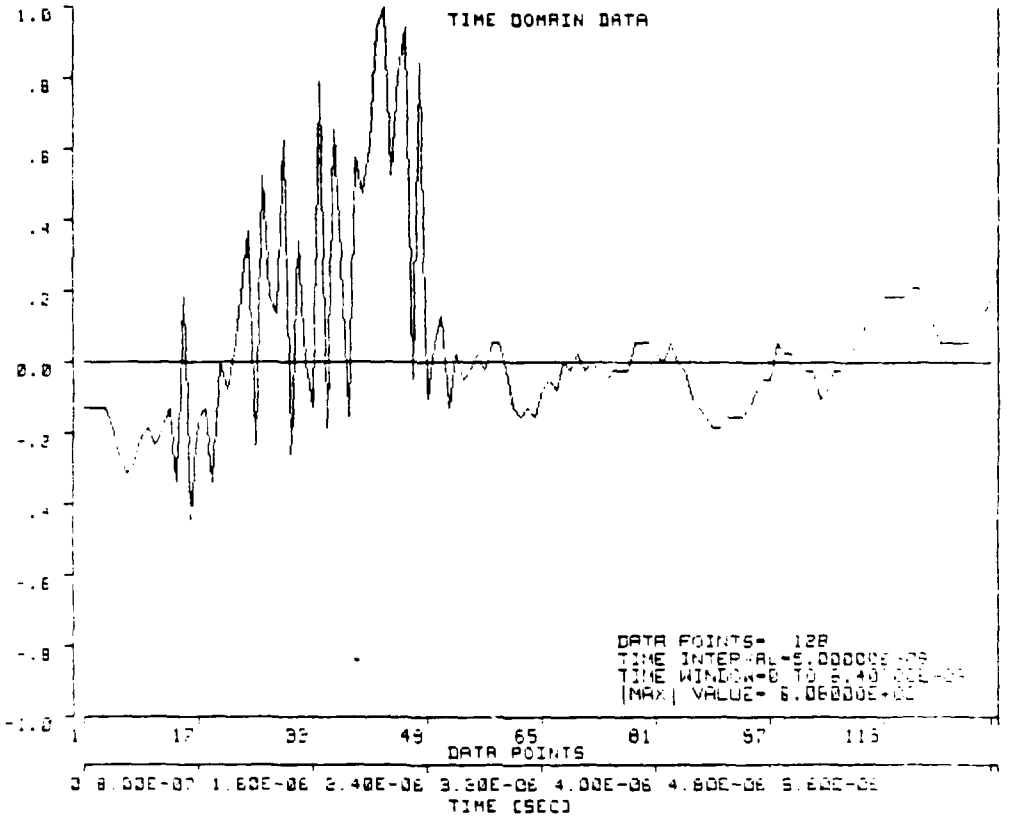

Figure 39. Type II Event Extracted from the Waveform Shown in Figure 37, for 304L SS

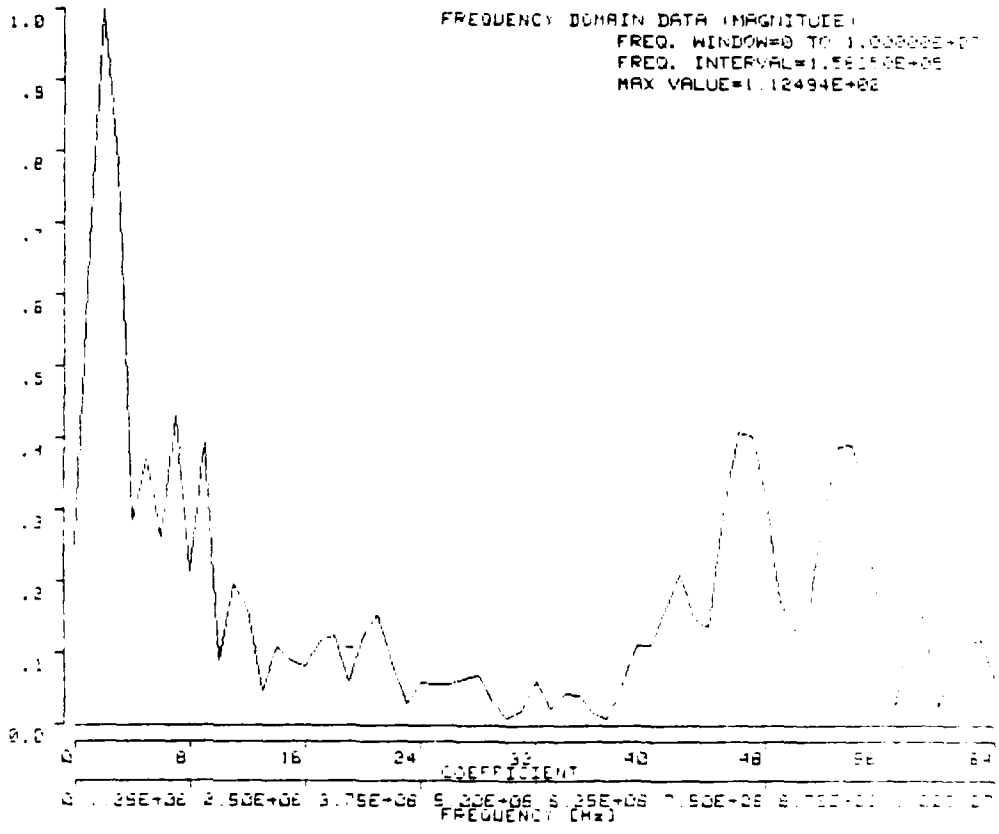

Figure 40. Frequency Spectrum of the Type II Event Shown in Figure 39, for 304L SS

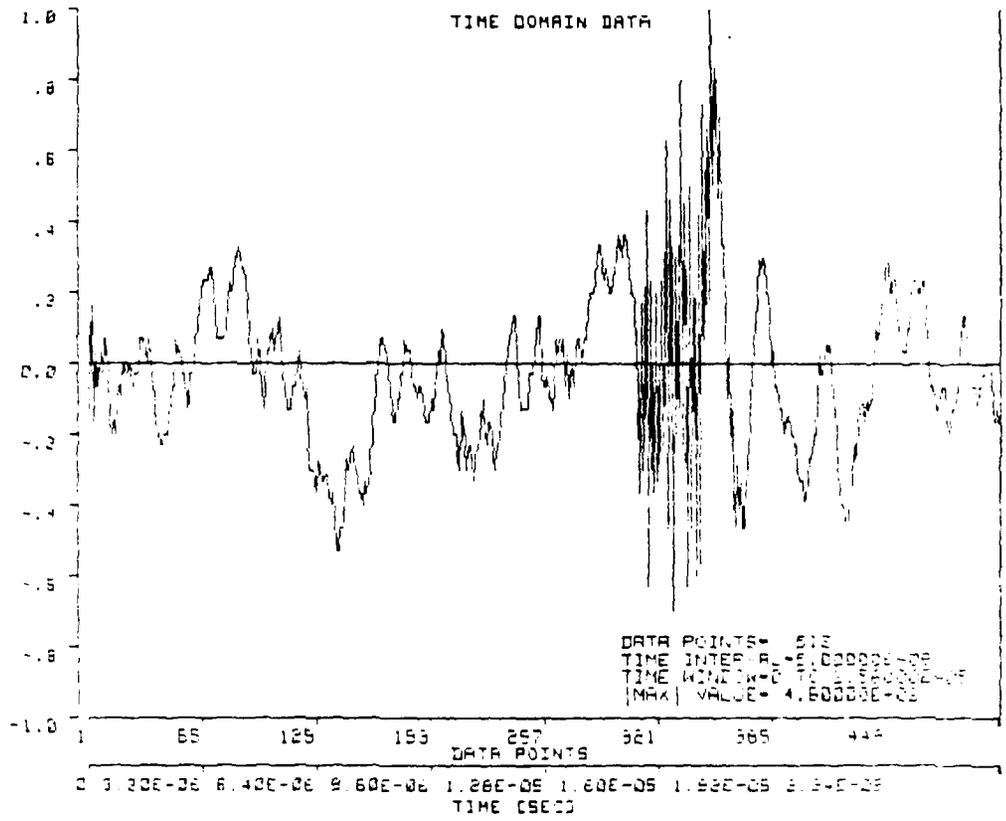

Figure 41. Type II Event Extracted from the Waveform Shown in Figure 37, for 304L SS

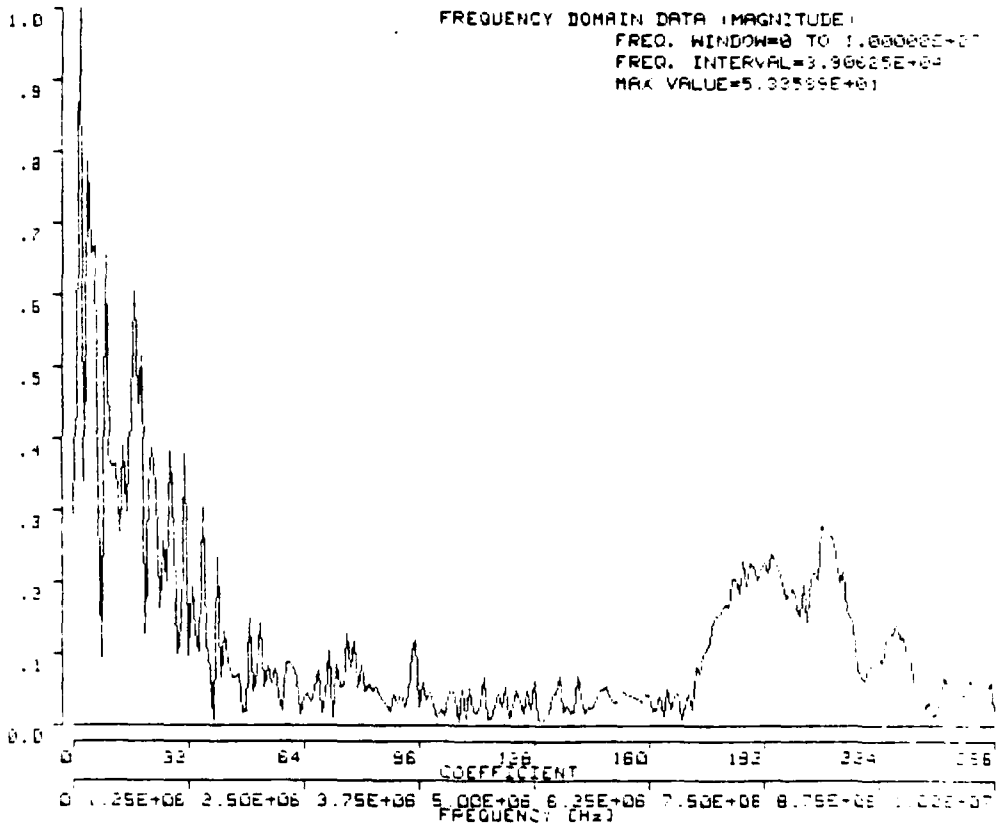

Figure 42. Frequency Spectrum of the Type II Event Shown in Figure 41, for 304L SS

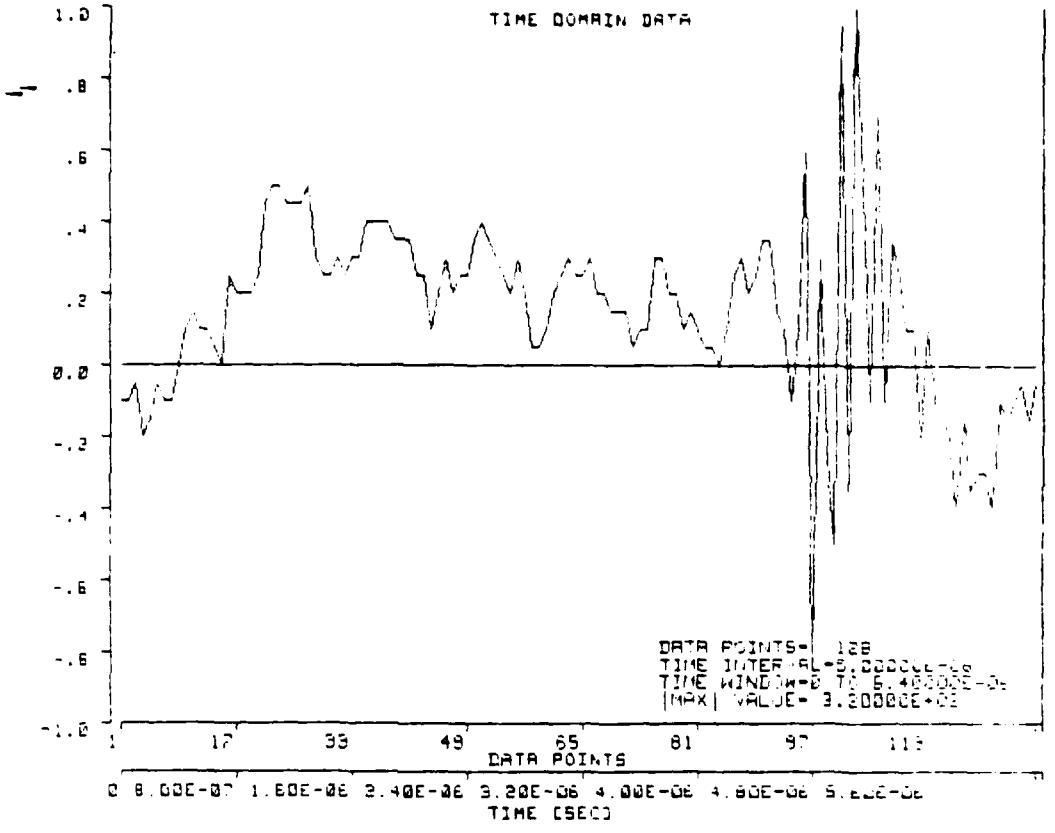

Figure 43. Type II Event Extracted from the Waveform Shown in Figure 37, for 304L SS

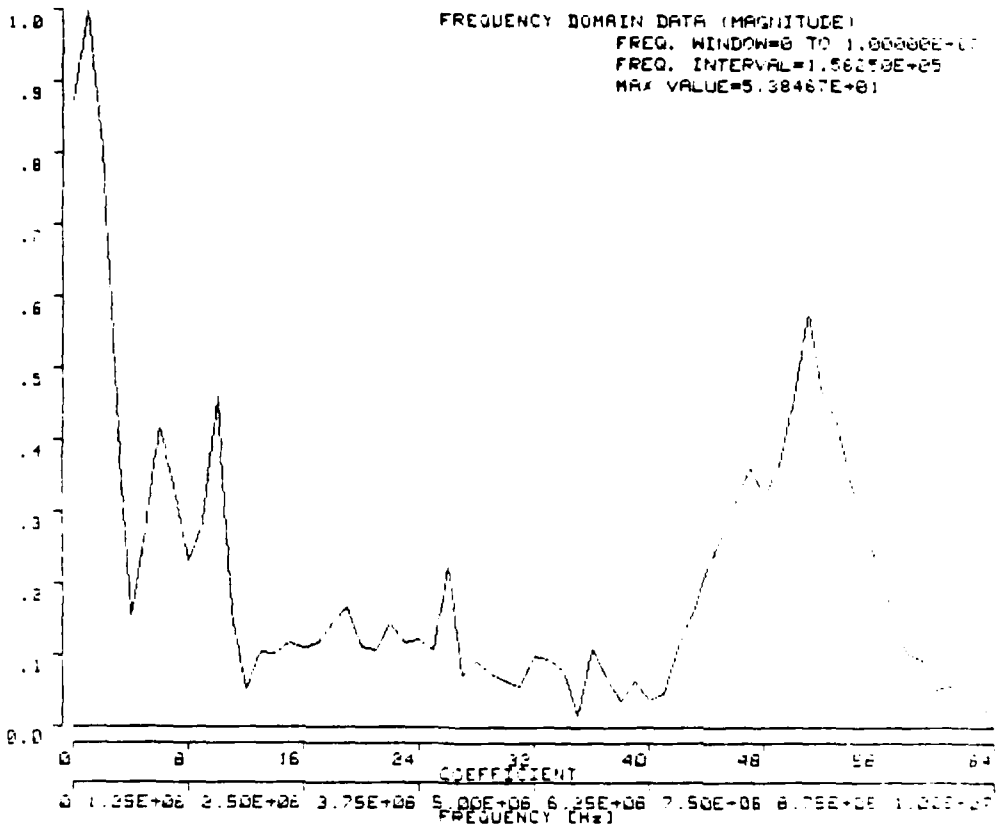

Figure 44. Frequency Spectrum of the Type II Event Shown in Figure 43, for 304L SS

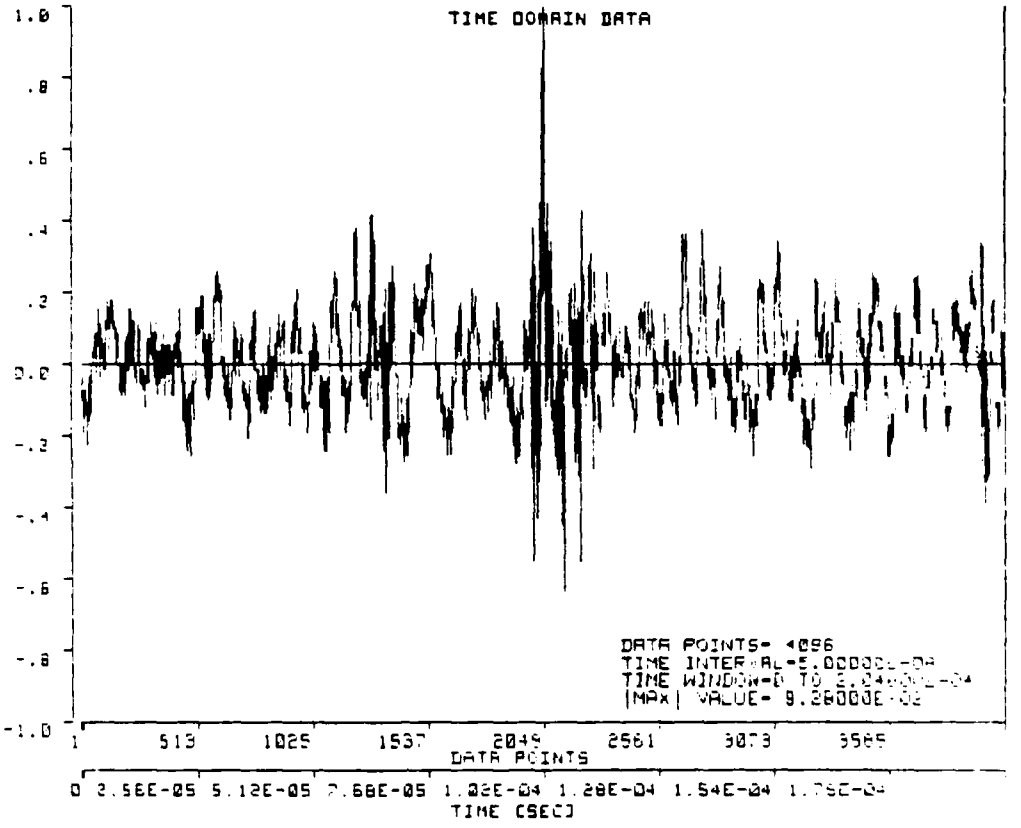

Figure 45. Typical Type II Waveform Observed During Deformation of a 304L SS Microtensile Specimen

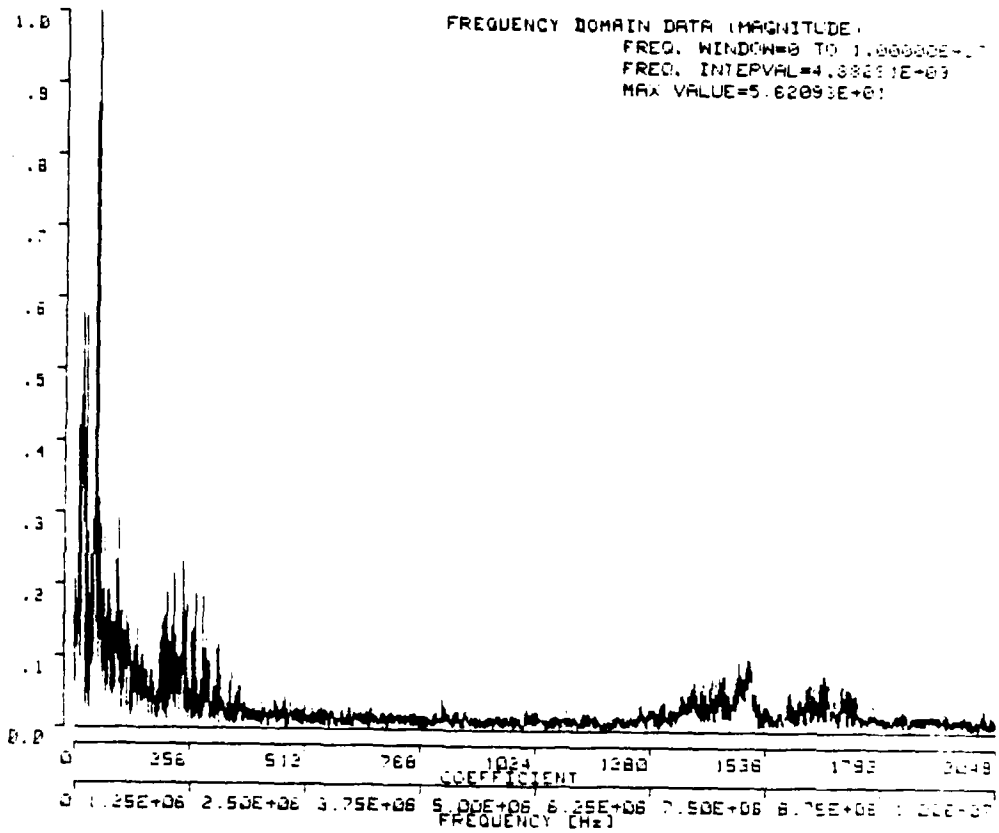

Figure 46. Frequency Spectrum of the Type II Waveform Shown in Figure 45, for 304L SS

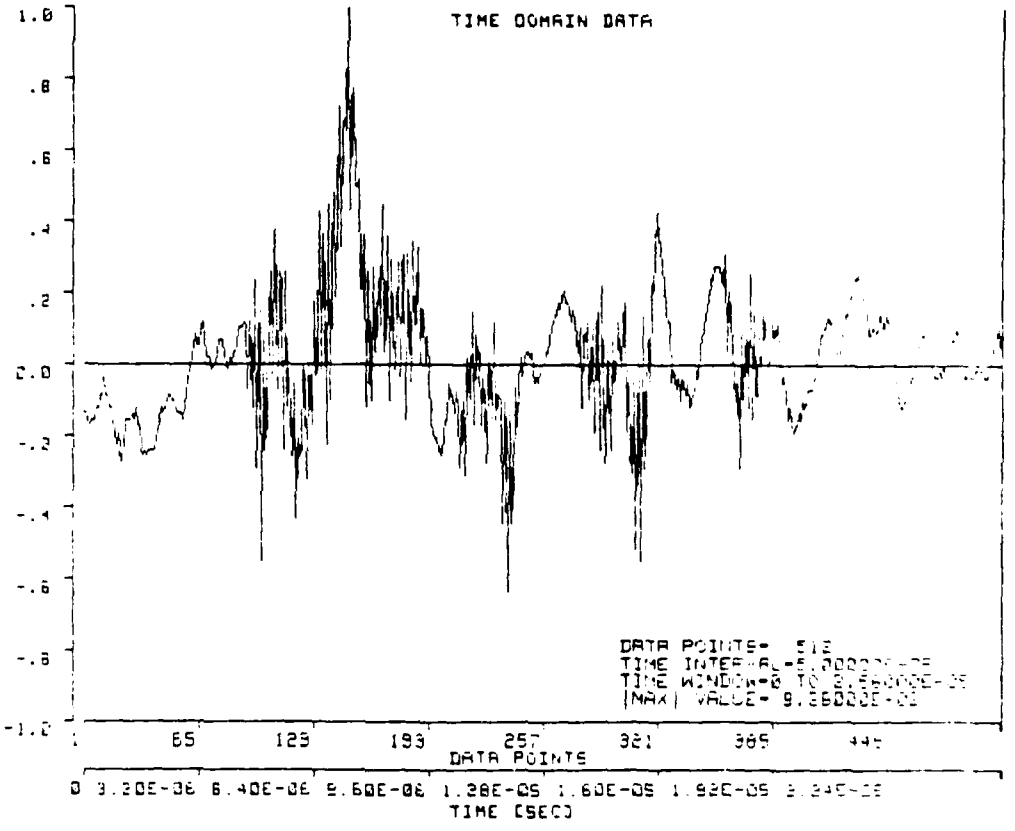

Figure 47. Typical Type II Event Extracted from the Waveform Shown in Figure 45, for 304L SS

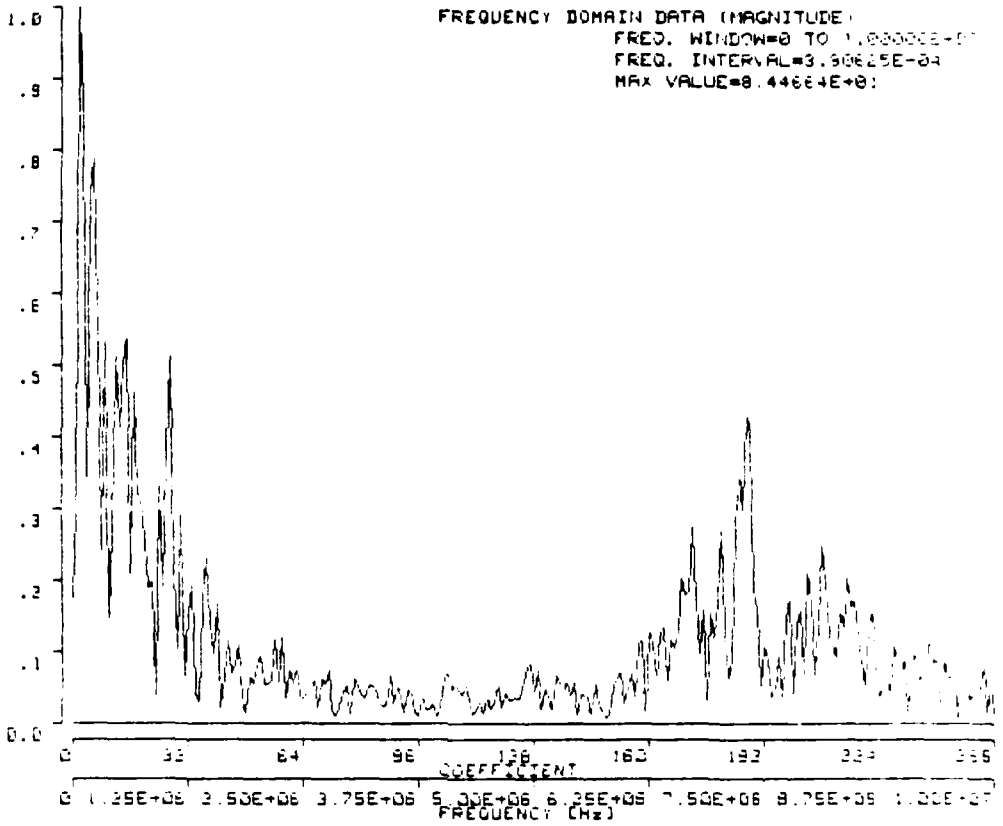

Figure 48. Frequency Spectrum of the Type II Event Shown in Figure 47, for 304L SS

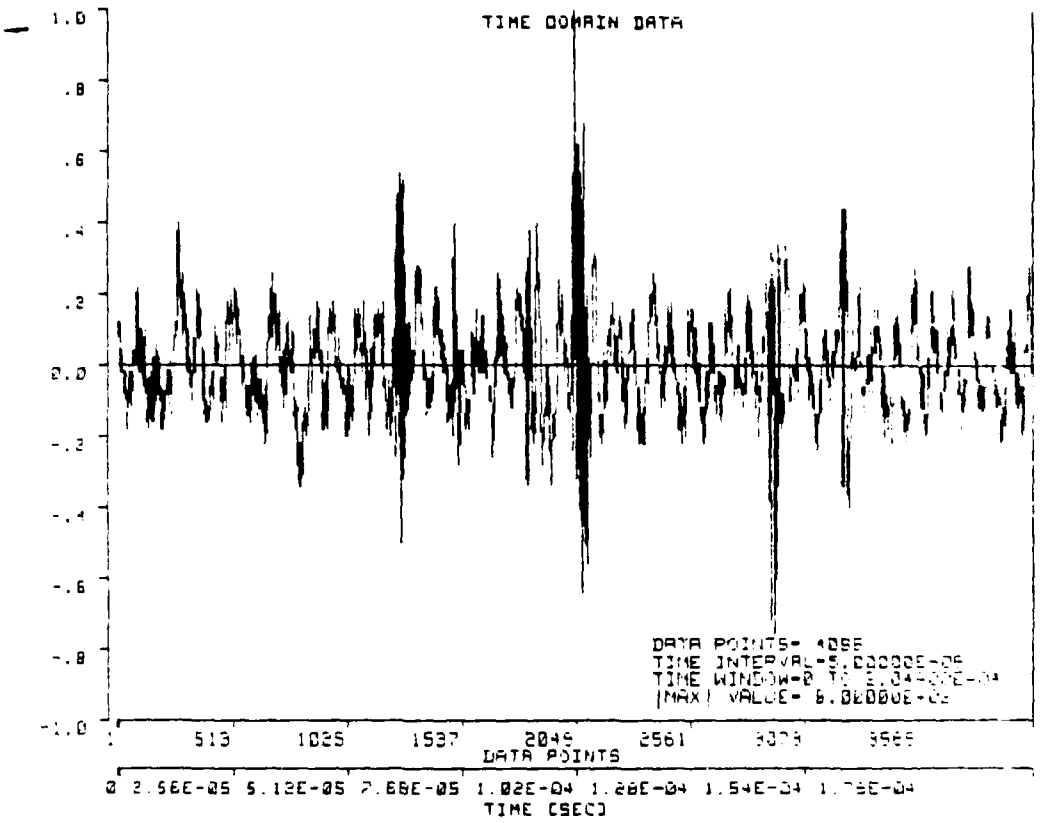

Figure 49. Typical Type II Waveform Observed During Deformation of a 304L SS Microtensile Specimen

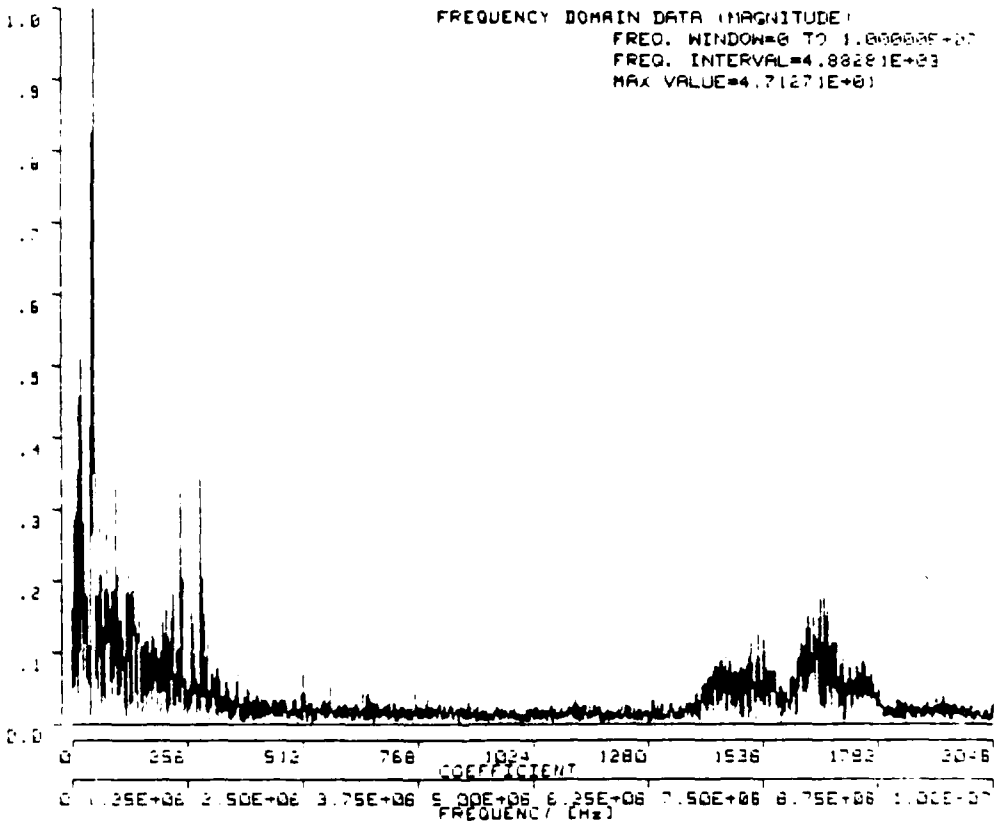

Figure 50. Frequency Spectrum of the Type II Waveform Shown in Figure 49, for 304L SS

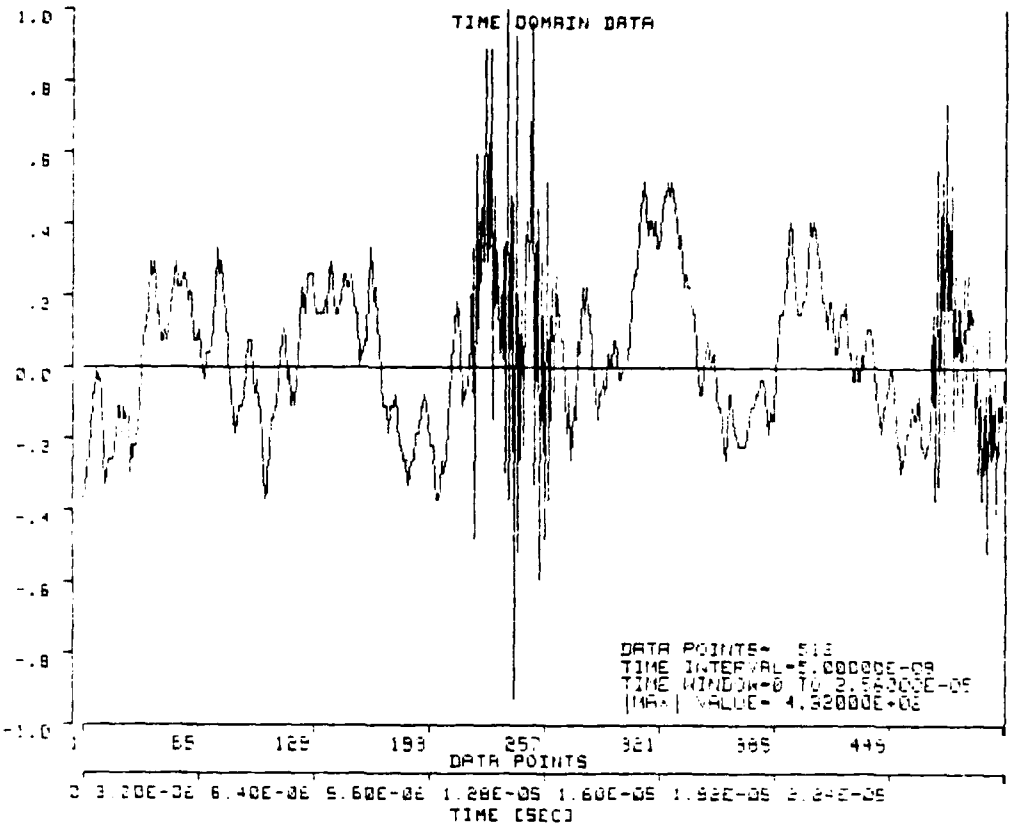

Figure 51. Type II Event Extracted from the Waveform Shown in Figure 49, for 304L SS

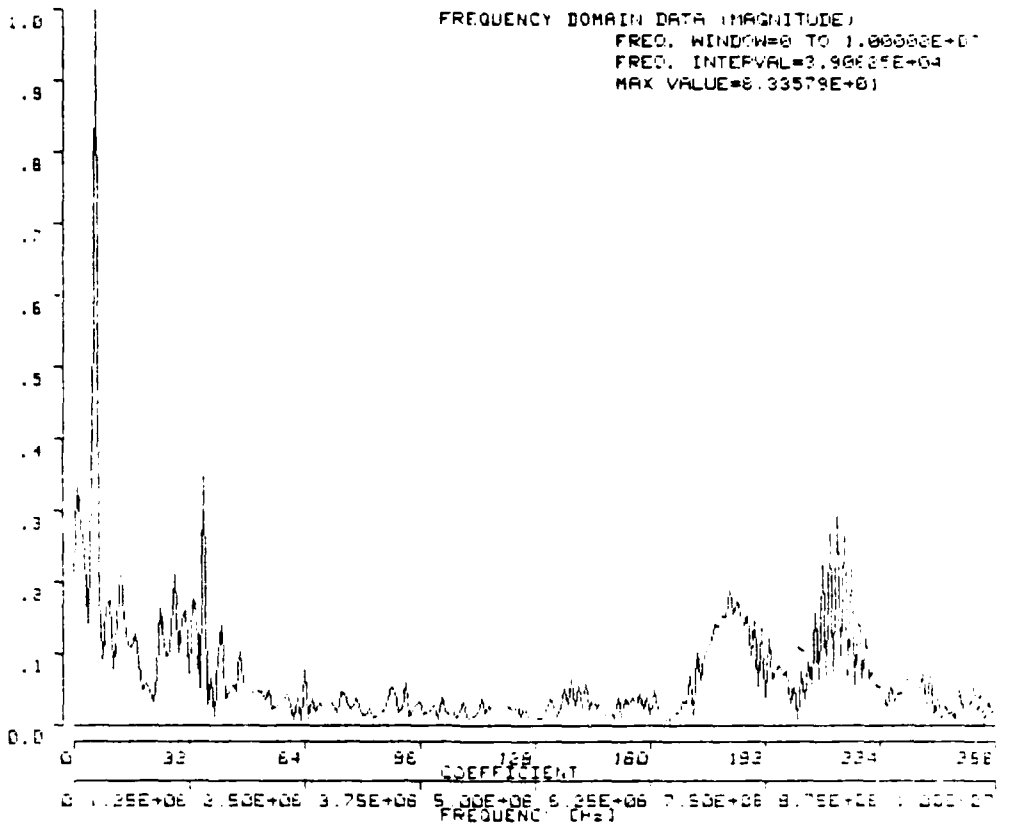

Figure 52. Frequency Spectrum of the Type II Event Shown in Figure 51, for 304L SS

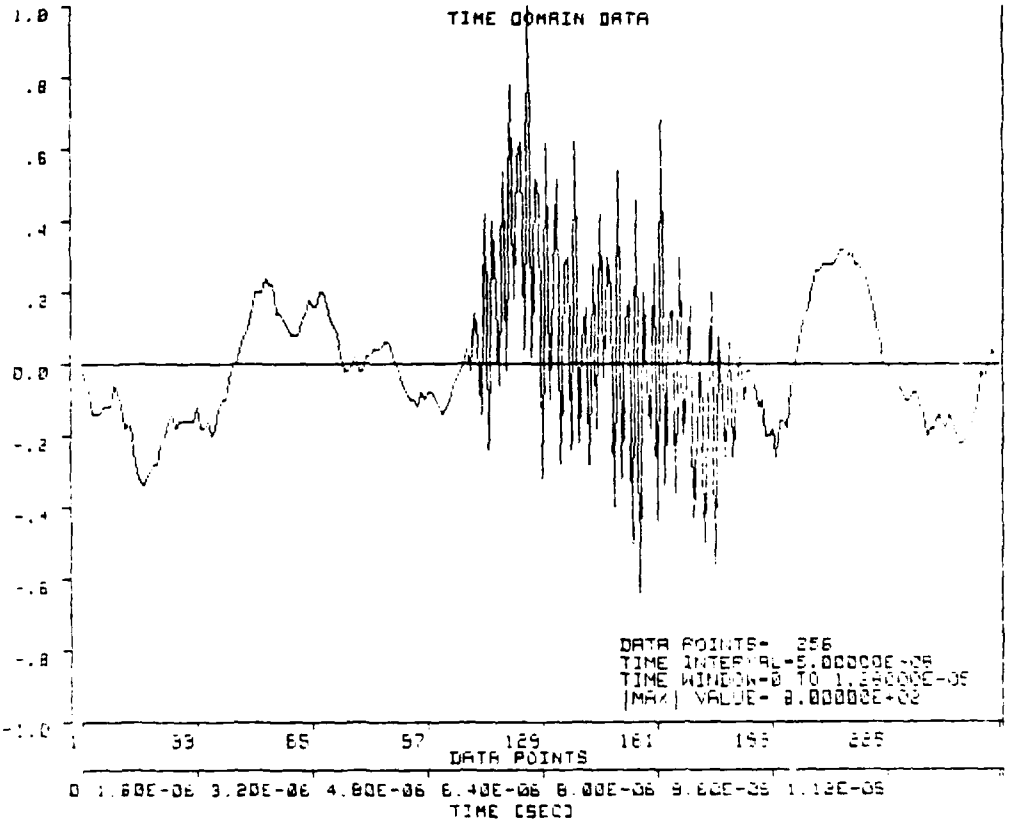

Figure 53. Type II Event Extracted from the Waveform Shown in Figure 49, for 304L SS

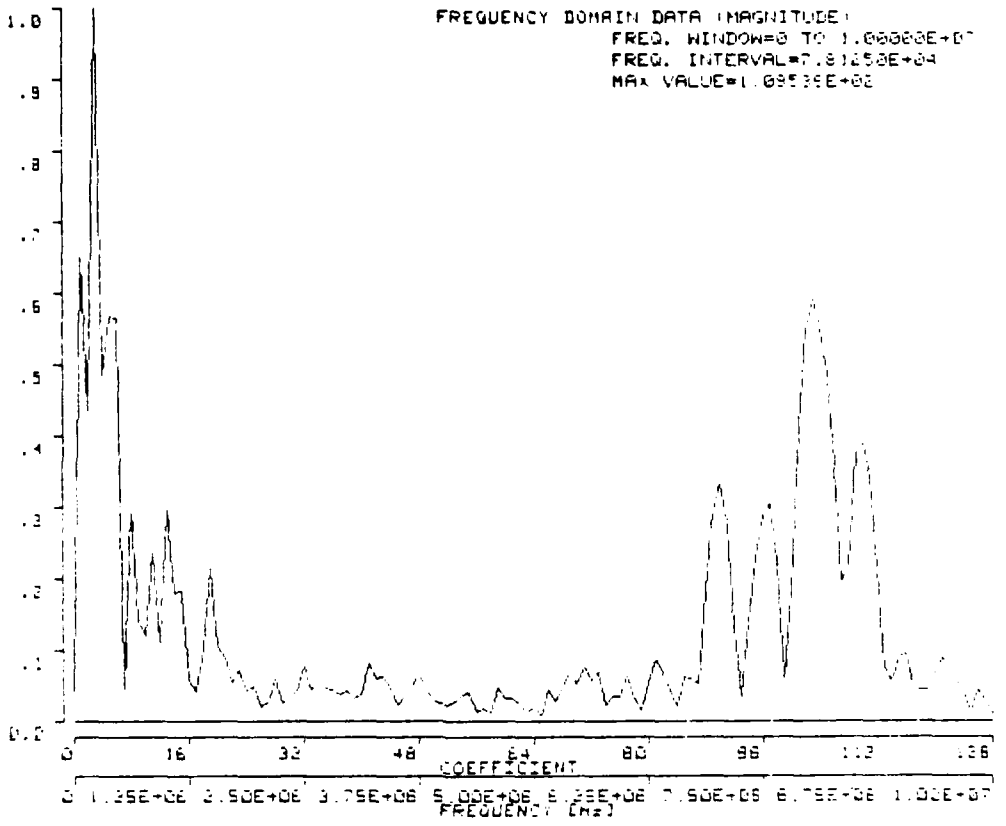

Figure 54. Frequency Spectrum of the Type II Event Shown in Figure 53, for 304L SS

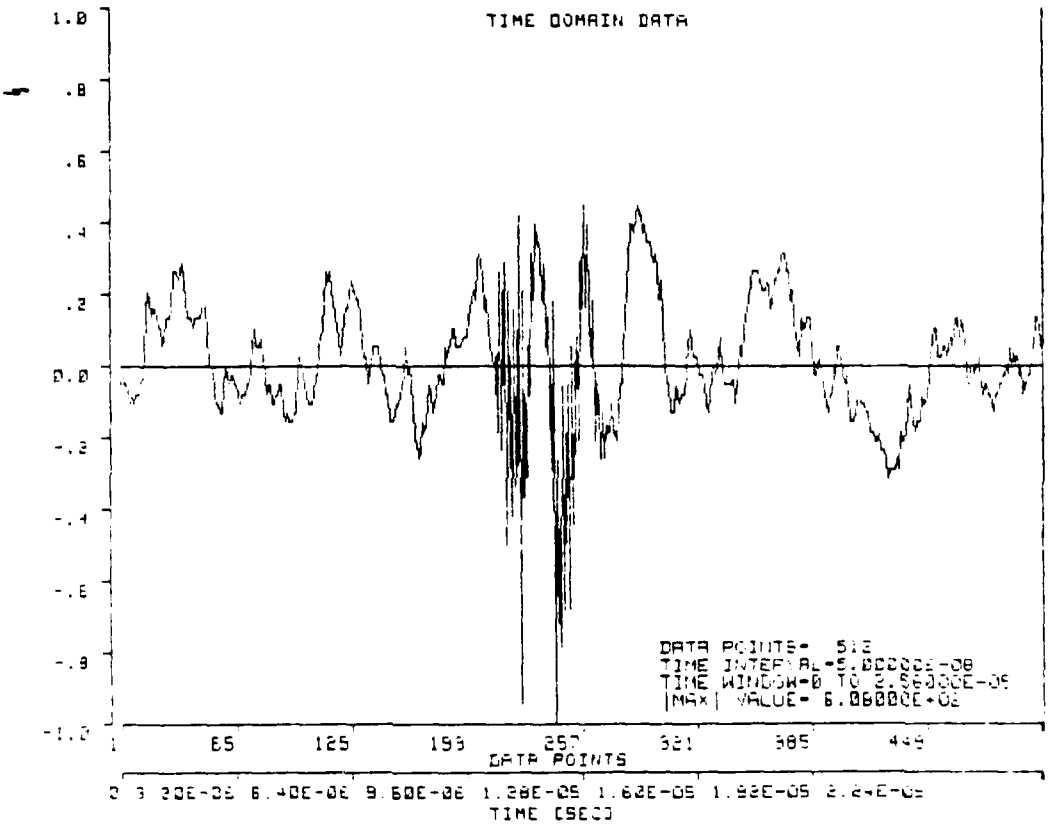

Figure 55. Type II Event Extracted from the Waveform Shown in Figure 49, for 304L SS

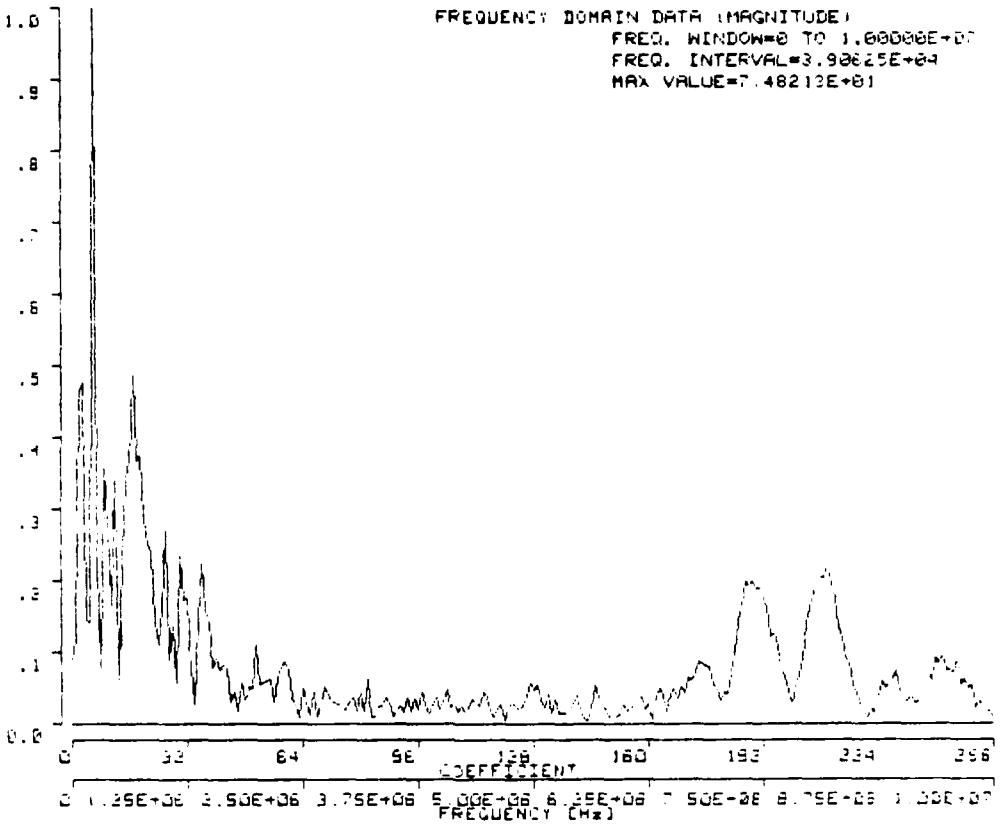

Figure 56. Frequency Spectrum of the Type II Event Shown in Figure 55, for 304L SS

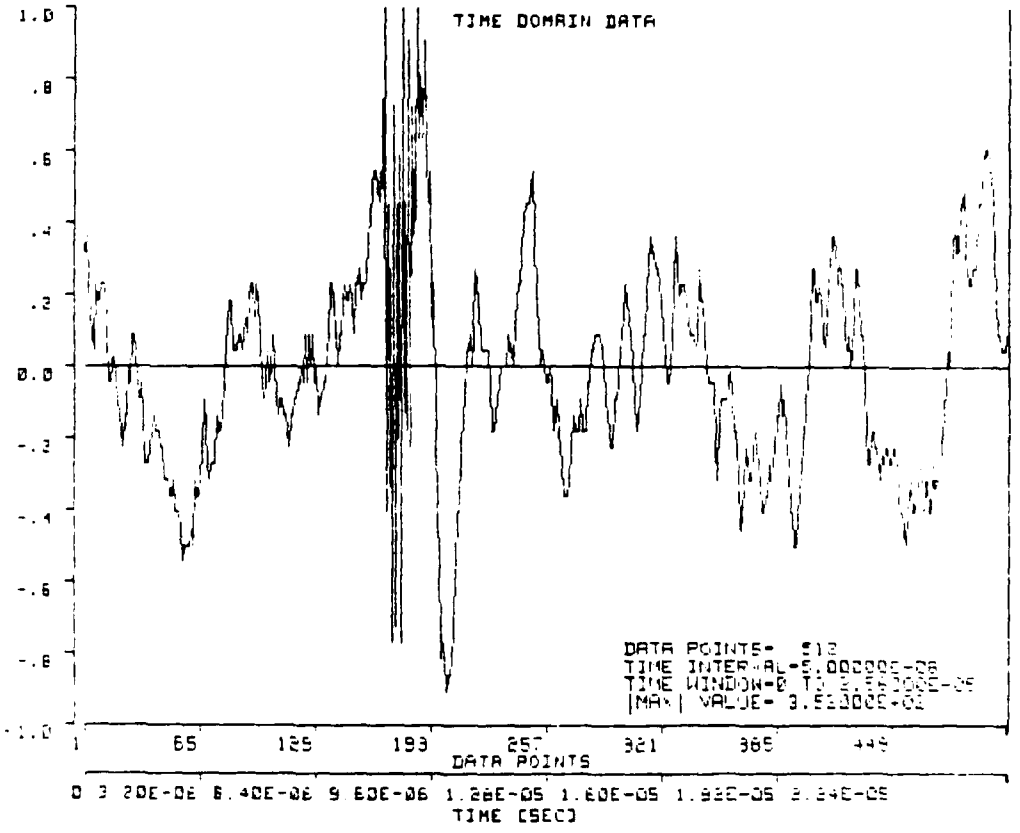

Figure 57. Type II Event Extracted from the Waveform Shown in Figure 49, for 304L SS

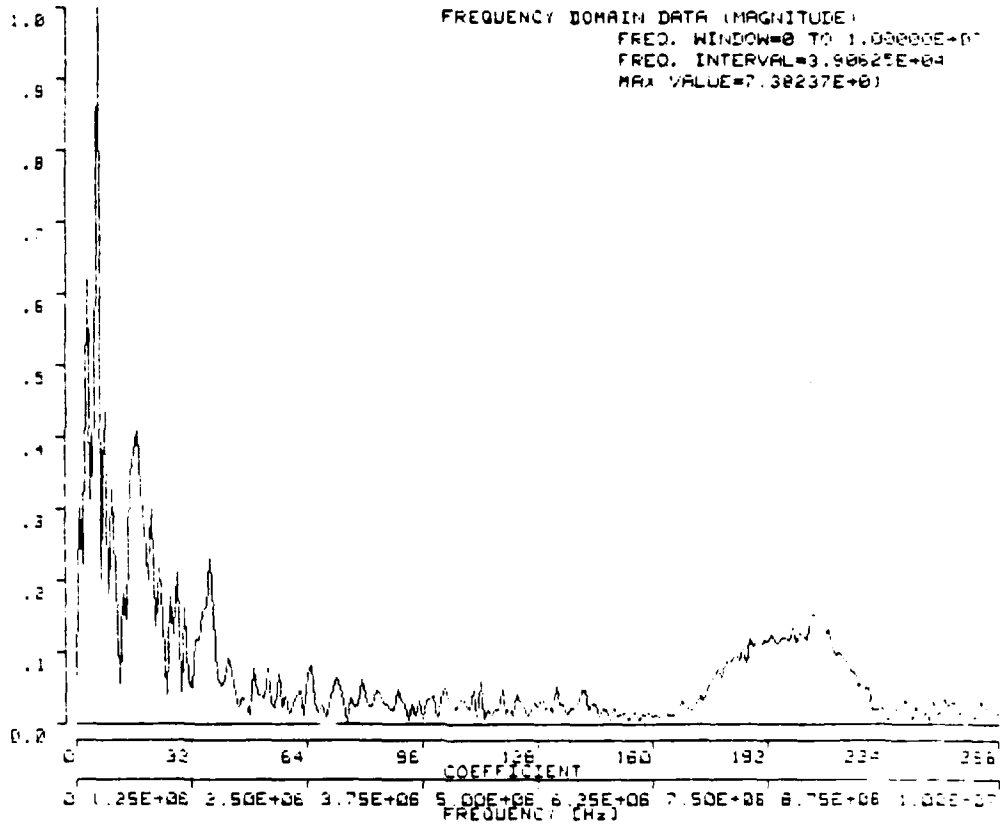

Figure 58. Frequency Spectrum of the Type II Event Shown in Figure 57, for 304L SS

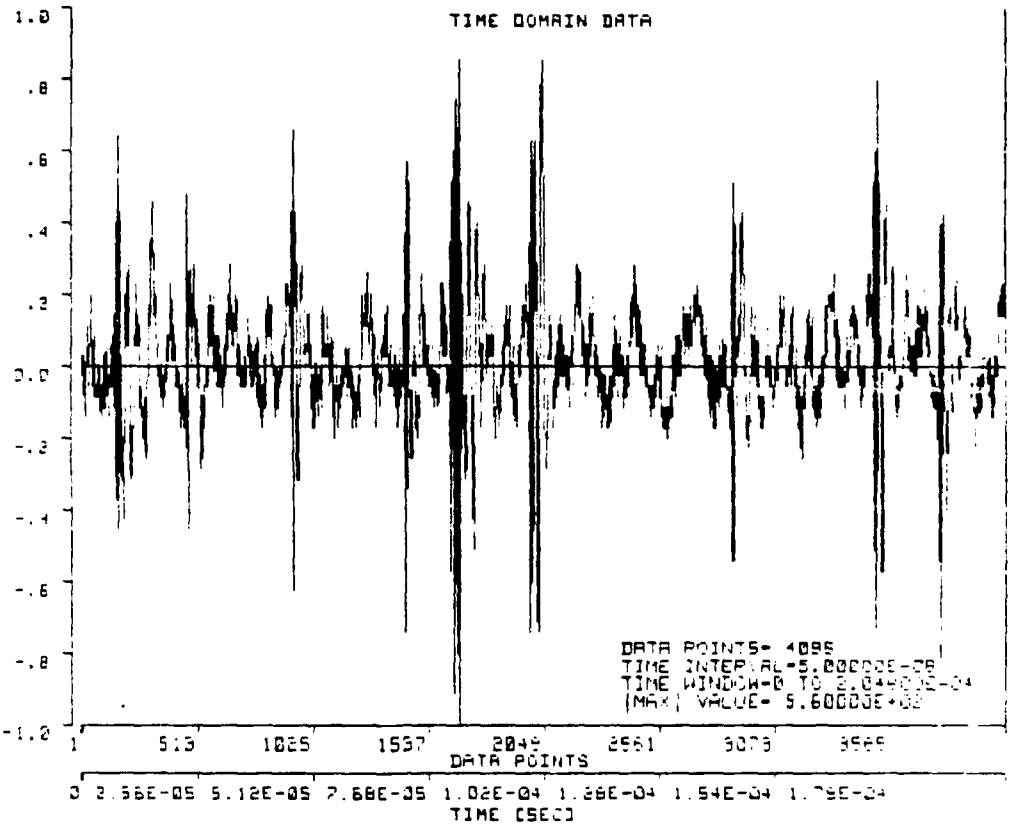

Figure 59. Typical Type II Waveform Observed During Deformation of a 304L SS Microtensile Specimen

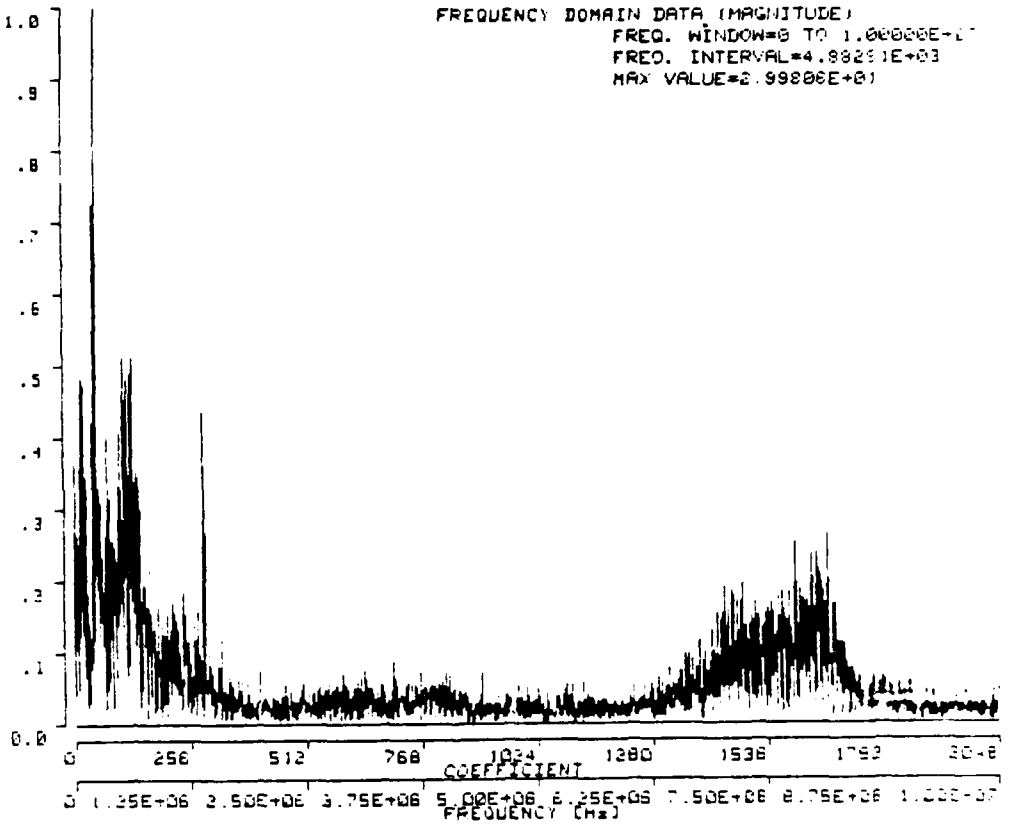

Figure 60. Frequency Spectrum of the Type II Waveform Shown in Figure 59, for 304L SS

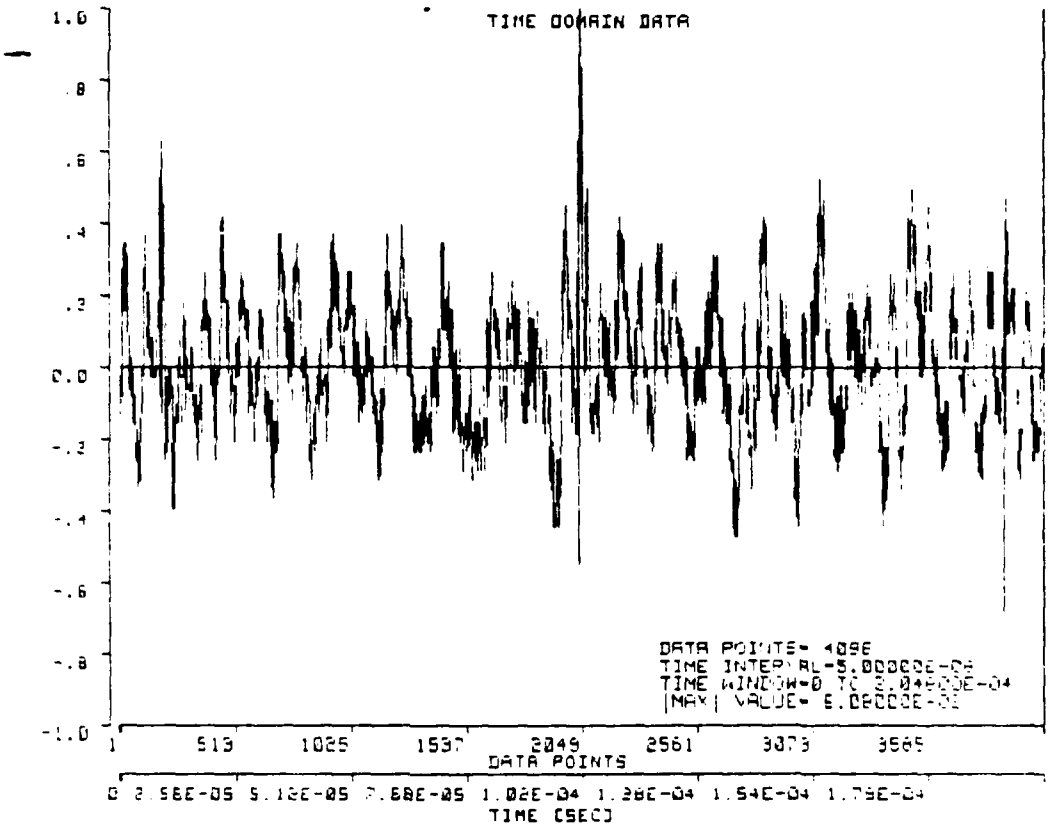

Figure 61. Typical Type II Waveform Observed During Deformation of a 304L SS Microtensile Specimen

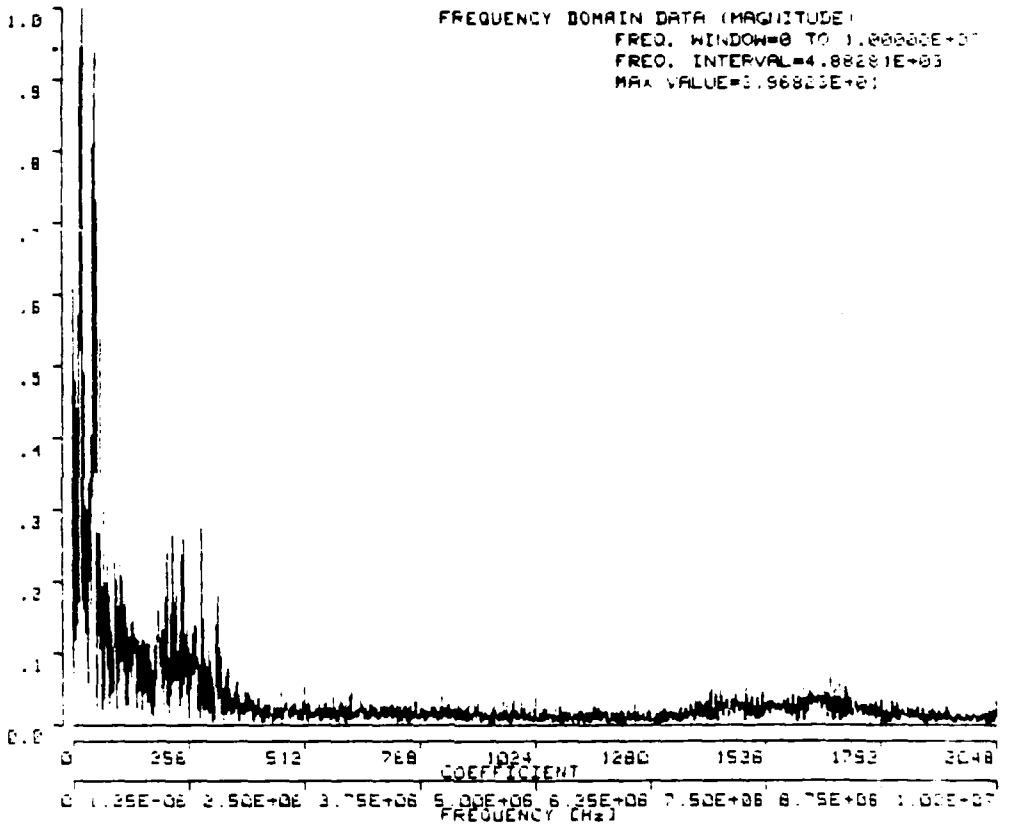

Figure 62. Frequency Spectrum of the Type II Waveform Shown in Figure 61, for 304L SS

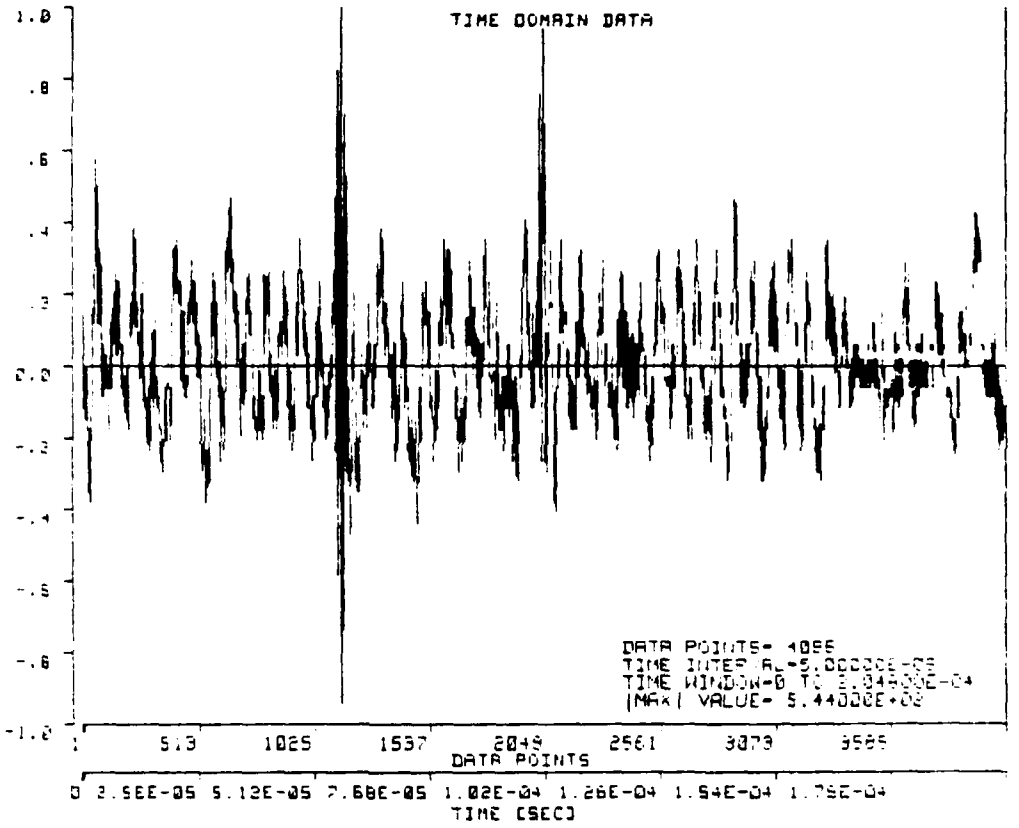

Figure 63. Typical Type II Waveform Observed During Deformation of a 304L SS Microtensile Specimen

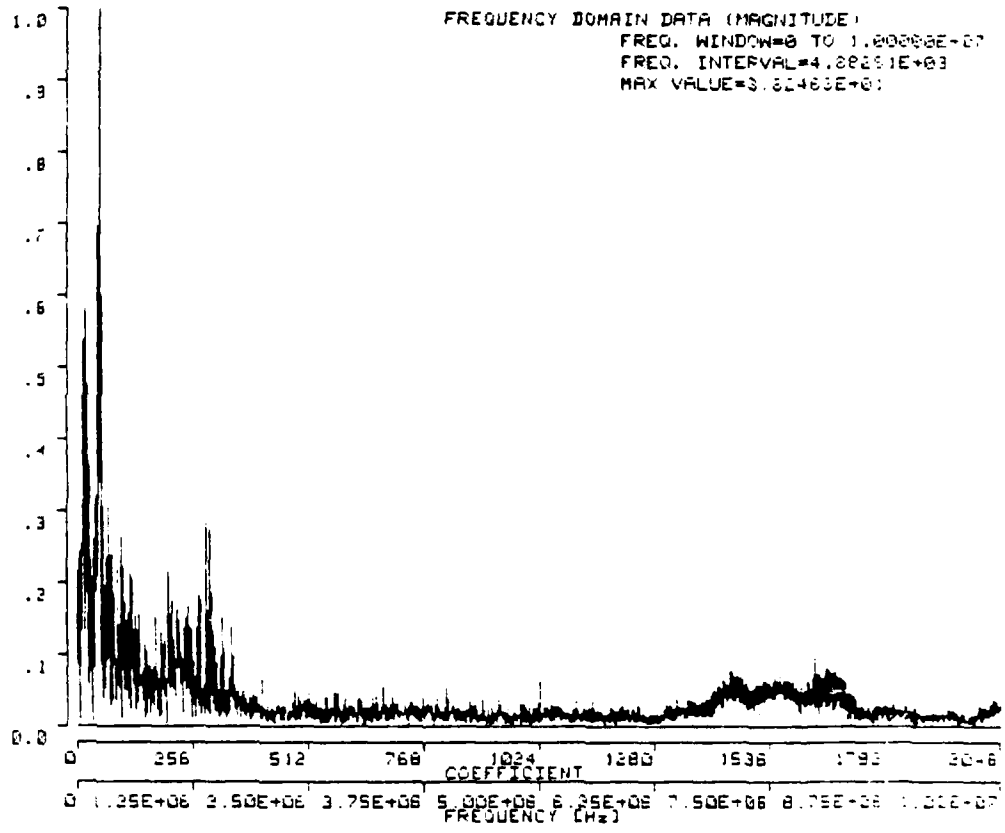

Figure 64. Frequency Spectrum of the Type II Waveform Shown in Figure 63, for 304L SS

engineering specimen, the signals may be attenuated sufficiently to not be observable.

The occurrence of the Type I and II events were compared to the load vs. time curves. The Type I events occurred uniformly randomly over the full loading cycle with a much greater frequency of occurrence than the Type II event. They were not concentrated either in the pre-yield or post-yield regimes. The Type II event was concentrated in the transition region between elastic and fully plastic deformation. Figure 65 shows the bounds within which the Type II events were witnessed superimposed on the average stress-strain diagram. In all the tests, there was no sudden increase in emissions just prior to failure. Each specimen died a quiet death.

One other important point should be mentioned. There was no evidence of continuous type acoustic emission signals. Both the Type I and II events would be classically described as burst type emissions.

During the examination of the fracture surfaces of the specimens, a count was made of the number of fractured particles located in the voids. Only the larger particles exhibited fracture. The smaller particles decohered from the matrix and remained intact. A direct count of the number of fractured particles showed a near one-to-one correspondence of fractured particle count and the number of Type II emissions. The number of emissions was always slightly less than the particle count.

IV. DISCUSSION

The results of this study on the tensile plastic deformation of a material differ from the observations of other investigators.[16 22 23] Two distinct signals, as distinguished by their waveforms, were observed. The Type I emission occurred uniformly throughout the tensile deformation of the material. The Type II emissions, with relatively high energy and high frequency content occurred in the transition region between elastic and fully plastic behavior.

Perhaps the best way to determine the source(s) of the signals is to first eliminate certain mechanisms and to then concentrate on the remaining candidates. The first item to discuss is the possibility that the optical probe is responding to resonant frequencies of the rectangular gage section. Calculations of resonant frequencies showed that the lowest resonance is at approximately 600 KHz and the next highest at 1.1 MHz.[24] The predominant frequencies of the Type I signal are about one-half the lowest resonance. In some of the test samples and signals captured, there did appear to be a frequency peak in the 1.1-1.2 MHz range suggesting that this was due to reverberations in the specimen. The 7.5-8.5 MHz frequencies of the Type II signal

---

[22] *K. Ono, H. Ucisik, "Acoustic Emission Behavior of Aluminum Alloys," UCLA Report ENG-7514, 1975.*

[23] *R. A. Kline, PhD. Thesis, Johns Hopkins Univ., 1978.*

[24] *L. Kinsler, A. R. Frey, Fundamentals of Acoustics, 2nd Ed., John Wiley Publ., New York, 1962.*

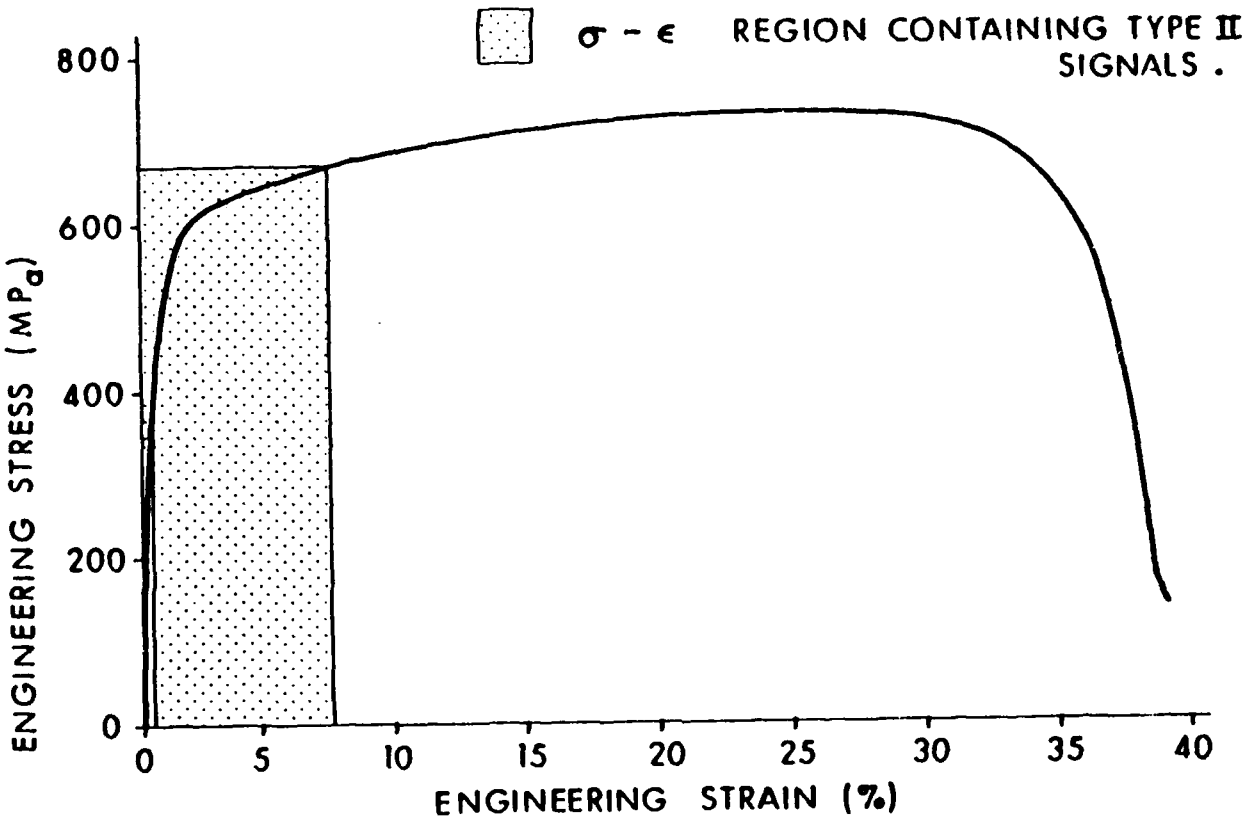

Figure 65. Stress-strain Curve for 304L SS Showing the Region in Which Type II Emissions Were Observed

would be such highorder harmonics that their magnitude would be inconsistent with the observed data.

Another possible source is slip band formation. The number of slip bands observed was far too large to be reconciled with the total number of Type I and II signals received. In an FCC material, no twinning would be expected and none was observed. The comment applying to the slip bands is also true for dimple formation and void coalescence (or ligament failure). They were just too numerous to reconcile with the observed counts. Additionally, voids coalescence could be observed in the final stage of deformation, but there was no increase in acoustic emission activity. Crack growth can also be eliminated. No evidence of crack growth was found either during tensile loading, after specimen examination just prior to failure or during fractographic examination after failure. Temperatures and strain rates were not such that any phase transformations would be expected.

The motion of mobile dislocations can also be ruled out as a likely candidate to produce the signals. The elastic strain energy of a dislocation responds very slowly to changes in the dislocation's position in the crystal except at positions very close to other defects. The energy can only change rapidly for defects in close proximity and suggests one of the most likely sources of emission is from dislocation pileups.[25]

The extensive grain boundary sliding which was observed can also be ruled out as a source. Acoustic emission generation requires the rapid release of energy. There was no evidence that the grain boundary motion was rapid. The view is also supported by other authors.[26] [27] [28] [29]

The two remaining mechanisms left are fracture of brittle intermetallic particles and dislocation pileup/unpinning. It is proposed that the Type II emissions are associated with fracturing of the intermetallics. This is supported by the correspondence between event counts and fractured particle count and the relatively high frequency of the emission. It would be expected that the fracture of a brittle particle on the order of 10μ diameter would emit short duration high frequency signals consistent with the observations. Fracture of intermetallics have been offered by a number of authors in a number of

---

[25] *P. P. Gillis, Mat. Res. and Stds., Vol. 11, No. 3, P. 11, 1971.*

[26] *R. Frydman, R. Pascual, R. M. Volpi, Scripta Met., Vol. 9, p. 1267, 1975.*

[27] *T. Malis, K. Tangri, Acta Met., Vol. 27, p. 25, 1979.*

[28] *K. N. Tandon, K. Tangri, Mat. Sci. and Engin., 20, p. 47, 1975.*

[29] *K. N. Tandon, K. Tangri, Mat. Sci. and Engin., 29, p. 37, 1977.*

materials as the source of emissions.[30-32] This is believed to be the first time that direct counts, rather than statistical counts, and the unique frequency spectrum support this hypothesis.

It is proposed that the Type I emissions are due to dislocation pile-up breakaway. Any number of sites are present to produce these pile-ups such as grain boundary triple points, inclusions, intermetallics, interstitials, etc. Based on the work carried out thus far, it cannot be stated unequivocably which microstructural feature is the source of the breakaway. Plausibility arguments can be given for each feature. The existence of the Type I spectrum within the Type II spectrum also supports Type I emissions being due to dislocation breakaway. Fracture of the intermetallics would most likely release sufficient energy to allow for the pileups to break away.

The last point to be discussed is the absence of a continuous type acoustic emission signal. It is felt that a major source of these emissions is the rapid motion of great numbers of dislocations into a region of large strain energy providing a local relaxation in that region. In other words, while a few dislocations are not of sufficient energy to be detected, the cascading effect of the motion of great numbers would be. It is felt that the same size of the tensile specimens used, limit the number of these dislocations to the extent that their motion cannot be detected. Follow-on experiments should be run varying specimen gage volume to determine if this hypothesis is correct.

V. CONCLUSIONS

This work has dealt with the acoustic emission behavior of 304L stainless steel during tensile deformation. The utility of studying acoustic emission using an optical probe and a micro-tensile specimen was demonstrated. Analysis of the signals received during deformation revealed the presence of two different waveforms. One containing a heretofore unobserved 7.5-8.5 MHz frequency component due to fracture of intermetallic particles. The other, a low frequency signal in the kilohertz range were believed due to breakaway of dislocation pileups. The ability to decern these two signals was due to the broad flat frequency response of the optical probe and the ability to probe immediately adjacent to the source by using extremely small gage sections in tensile specimens. The combination of optical probing of microtensile specimens provides a new unique and powerful tool for studying the mechanisms of acoustic emission.

---

[30] *R. Bianchetti, M. A. Hamsted, A. K. Mukherjee, J. of Testing and Evaluation, Vol. 3, No. 3, p. 167, 1975.*

[31] *S. H. Goods, L. M. Brown, Acta Met., Vol. 27, p. 1, 1979.*

[32] *W. W. Gerberich, M. Stout, K. Jatavallabhula, D. Atteridge, Int. J. of Frac., Vol. 15, No. 6, p. 491, 1979.*

REFERENCES

1. J. Kaiser, PhD. Thesis, Tech. Hochsch., Munchen (1950).

2. B. H. Schofield, AF 33(616)-5640, Lessells and Associates, Int., Boston, 1960.

3. B. H. Schofield, Proc. of Symposium on Physics and Non-Destructive Testing, 63-82, 1963.

4. R. G. Liptai, D. O. Harris, R. B. Engle, C. A. Tatro, Inc. J. of NDT, Vol. 3, 215-275, 1971.

5. H. L. Dunegan, A. S. Tetleman, Research/Development, May 1971, p. 20.

6. A. E. Lord, "Physical Acoustics," W. P. Mason and R. N. Thurston (Editors), Vol. 11, p. 289, 1975.

7. A. A. Pollock, Acoustics and Vibration Progress, R. W. B. Stephens and H. G. Leventhall (Editors), Vol. 1, p. 53-84, 1974.

8. P. H. Hutton, R. N. Ord., "Acoustic Emission", R. S. Sharpe (Editor), Research Techniques in NDT, p. 1-30, 1970.

9. R. G. Liptai, D. O. Harris, C. A. Tatro (Editors), ASTM STP 505, ASTM, Phila., Pa., 1972.

10. J. C. Spanner, Acoustic Emission, Techniques and Applications, INTEX Publ. Co., Evanston, Ill., 1974.

11. A. E. Lord, Physical Acoustics, W. P. Mason and R. N. Thurston (Editors), Vol. 11, p. 289, 1975.

12. J. C. Spanner, J. W. McElroy (Editors), Monitoring Structural Integrity by Acoustic Emission, ASTM STP 571, ASTM, 1975.

13. M. Arrington, British J. of NDT, 17, p. 10, 1975.

14. H. N. G. Wadley, C. B. Scruley, Acta. Met., Vol. 27, p. 613, 1979.

15. S. E. Fick, C. H. Palmer, Applied Optics, Vol. 17, No. 17, p. 2686, 1978.

16. R. A. Kline, R. E. Green, C. H. Palmer, J. Acoust. Soc. Am., 64(6), 1978.

17. C. H. Palmer, S. E. Fick, Proc. of Southeastcon '79, p. 191, 1979.

18. C. H. Palmer, R. E. Green, "Optical Probing of Acoustic Emission Waves," Final Report, U.S. Army Research Office, North Carolina, 1979.

19. D. R. James, S. H. Carpenter, Scripta Met., Vol. 10, p. 779, 1976.

20. W. C. Rion, "Stainless Steel Information Manual for the Savannah River Plant", Vol. 1, Dupont Report DP-860, 1964.

21. B. W. Christ, S. R. Swanson, J. of Test and Eval., Vol. 4, No. 6, p. 405, 1976.

22. K. Ono, H. Ucisik, "Acoustic Emission Behavior of Aluminum Alloys," UCLA Report ENG-7514, 1975.

23. R. A. Kline, PhD. Thesis, Johns Hopkins Univ., 1978.

24. L. Kinsler, A. R. Frey, Fundamentals of Acoustics, 2nd Ed., John Wiley Publ., New York, 1962.

25. P. P. Gillis, Mat. Res. and Stds., Vol. 11, No. 3, p. 11, 1971.

26. R. Frydman, R. Pascual, R. M. Volpi, Scripta Met., Vol. 9, p. 1267, 1975.

27. T. Malis, K. Tangri, Acta Met., Vol. 27, p. 25, 1979.

28. K. N. Tandon, K. Tangri, Mat. Sci, and Engin., 20, p. 47, 1975.

29. K. N. Tandon, K. Tangri, Mat. Sci. and Engin., 29, p. 37, 1977.

30. R. Bianchetti, M. A. Hamsted, A. K. Mukherjee, J. of Testing and Evaluation, Vol. 3, No. 3, p. 167, 1975.

31. S. H. Goods, L. M. Brown, Acta Met., Vpl. 27, p. 1, 1979.

32. W. W. Gerherich, M. Stout, K. Jatavallabhula, D. Atteridge, Int. J. of Frac., Vol. 15, No. 6, p. 491, 1979.

33. J. R. Frederick. D. K. Felbeck, "Acoustic Emission", ASTM STP 505, ASTM Phila, Pa., p. 129, 1972.

34. P. Neumann, Mat. Sci. and Engin, 25, p. 217, 1976.

35. J. Masounave, J. Lanteigne, M. N. Bassim, D. R. Hay, Engin. Frac. Mech., Vol. 8, p. 701, 1976.

36. M. A. Hamsted, R. Bianchetti, A. K. Mukherjee, Engin. Frac. Mech., Vol. 9, p. 665, 1977.

37. W. W. Gerherich, D. G. Atteridge, J. F. Lessar, Met. Trans. A, Vol. 6A, [illegible]

38. [illegible] Canadian J. of Phys., Vol. 45, p. 1147, 1967.

DISTRIBUTION LIST

No. of Copies	Organization
12	Administrator Defense Technical Info Center ATTN: DDC-DDA Cameron Station Alexandria, VA 22304-6145
1	Deputy Assistant Secretary of the Army (R&D) Department of the Army Washington, DC 20310
1	HQDA DAMA-ARP-P, Dr. Watson Washington, DC 20310
1	HQDA DAMA-ART-M Washington, DC 20310
1	HQDA DAMA-MS Washington, DC [illegible]
1	Commander US Army War College ATTN: Lib Carlisle Barracks, PA [illegible]
1	Commander US Army Command and General Staff College ATTN: Archives Fort Leavenworth, KS [illegible]
1	Commander US Army Material [illegible] ATTN: AMCPM-LCT [illegible] Eisenhower Ave Alexandria, VA [illegible]
1	Commander Armament R&D Center US Army AMCCOM ATTN: SMCAR-[illegible] [illegible]

No. of Copies	Organization
1	Commander Armament R&D Center US Army AMCCOM ATTN: SMCAR-TSS Dover, NJ 07801
1	Commander Benet Weapons Laboratory ATTN: Dr. E. Schneider Watervliet, NY 12189
1	Director Benet Weapons Laboratory Armament R&D Center US Army AMCCOM ATTN: SMCAR-LCB-TL Watervliet, NY 12189
1	Commander US Army Armament, Munitions and Chemical Command ATTN: SMCAR-ESP-L Rock Island, IL [illegible]
1	Commander US Army Aviation Research and Development Command ATTN: AMSAV-E 4300 Goodfellow Boulevard St. Louis, MO [illegible]
1	Director US Army Air Mobility Research and Development Command Ames Research Center Moffett Field, CA [illegible]
1	Commander US Army Communications- Electronics Command ATTN: AMSEL-[illegible] Fort Monmouth, NJ [illegible]

DISTRIBUTION LIST

No. of Copies	Organization
1	Commander US Army Harry Diamond Laboratory ATTN: DELHD-TA-L 2800 Powder Mill Road Adelphi, MD 20783
1	Commander MICOM Research, Development and Engineering Center ATTN: AMSMI-RD Redstone Arsenal, AL 35898
1	Director Missile and Space Intelligence Center ATTN: AIAMS-YDL Redstone Arsenal, AL 35898-5500
1	Director BMD Advanced Technology Center ATTN: ATC-T, M. Capps ATC-M, C. Brockway ATC-EN, P. Boyd P. O. Box 1500 Huntsville, AL [illegible]
1	[illegible] [illegible] [illegible] Arlington, VA [illegible]
1	[illegible] [illegible] [illegible] ATTN: [illegible] [illegible]
1	[illegible] [illegible] [illegible] ATTN: [illegible] [illegible]
1	Commander US Army Tank Automotive Command ATTN: AMSTA-TSL Warren, MI 48090
1	Commander US Army Electronics Proving Ground ATTN: Tech Lib Fort Huachuca, AZ 85613
3	Commander US Army Materials and Mechanics Research Center ATTN: AMXMP-T, J. Mescall AMXMR-T, R. Shea AMXMR-H, S.C. Chou Watertown, MA 02172
1	Director US Army TRADOC Systems Analysis Activity ATTN: ATAA-SL White Sands Missile Range, NM [illegible]
1	[illegible] [illegible] [illegible] ATTN: [illegible] [illegible]
1	[illegible] [illegible] [illegible] ATTN: [illegible] [illegible]
1	[illegible] [illegible] [illegible] ATTN: [illegible] [illegible]

DISTRIBUTION LIST

No. of Copies	Organization
1	Commander US Army Development and Employment Agency ATTN: MODE-TED-SAB Fort Lewis, WA 98433
1	Office of Naval Research Department of the Navy ATTN: Code 402 Washington, DC 20360
1	Commander Naval Surface Weapons Center ATTN: Code Gr-9, Dr. W. Soper Dahlgren, VA 22448
1	Commander and Director US Naval Electronics Laboratory San Diego, CA 92152
5	Commander US Naval Research Laboratory ATTN: C. Sanday R. J. Weimer Code 5270, F. MacDonald Code 2020, Tech Lib Code 7786, J. Baker Washington, DC 20375
1	AFATL (DLDG) Eglin AFB, FL 32542-5000
1	Air Force Armament Laboratory ATTN: AFATL/DLODL Eglin AFB, FL 32542-5000
1	AFATL (DLYW) Eglin AFB, FL 32542-5000
1	RADC (EMTLD, Lib) Griffiss AFB, NY 13440
1	AFWL/[illegible] Kirtland AFB, NM [illegible]
1	[illegible] Maxwell AFB, AL [illegible]
1	AFFDL/FB, Dr. J. Halpin Wright-Patterson AFB, OH 45433
5	Sandia National Laboratories ATTN: Dr. L. Davison Dr. P. Chen Dr. W. Herrmann Dr. C. Harness H.J. Sutherland Albuquerque, NM 87115
1	Dupont Experimental Labs ATTN: Mr. J. Lupton Wilmington, DE 19801
2	Forestal Research Center Aeronautical Engineering Lab. Princeton University ATTN: Dr. S. Lam Dr. A. Eringen Princeton, NJ 08540
1	IBM Watson Research Center ATTN: R. A. Toupin Poughkeepsie, NY 12601
2	SRI International ATTN: Dr. Donald R. Curran Dr. Lynn Seaman 333 Ravenswood Avenue Menlo Park, CA 94025
3	California Institute of Technology Division of Engineering and Applied Science ATTN: Dr. J. Mikowitz Dr. E. Sternberg Dr. J. Knowles Pasadena, CA 91102
1	Massachusetts Institute of Technology ATTN: Dr. R. Probstein 77 Massachusetts Avenue Cambridge, MA 02139

DISTRIBUTION LIST

No. of Copies	Organization
2	Southwest Research Institute Department of Mechanical Sciences ATTN: Dr. U. Kindholm Dr. W. Baker 8500 Culebra Road San Antonio, TX 78228
5	Brown University Division of Engineering ATTN: Prof. R. Clifton Prof. H. Kolsky Prof. A. Pipkin Prof. P. Symonds Prof. J. Martin Providence, RI 02912
3	Carnegie-Mellon University Department of Mathematics ATTN: Dr. D. Owen Dr. M. E. Gurtin Dr. B. D. Coleman Pittsburgh, PA 15213
2	Catholic University of America School of Engineering and Architecture ATTN: Prof. A. Durelli Prof. J. McCoy Washington, DC 20017
4	Cornell University Department of Theoretical and Applied Mechanics ATTN: Dr. Y. H. Pao Dr. G. S. S. Ludford Dr. A. Ruoff Dr. J. Jenkins Ithaca, NY 14850
1	Harvard University Division of Engineering and Applied Physics ATTN: Dr. G. Carrier Cambridge, MA 02138
2	Iowa State University Engineering Research Laboratory ATTN: Dr. G. Nariboli Dr. A. Sedov Ames, IA 50010
2	Lehigh University Center for the Application of Mathematics ATTN: Dr. E. Varley Dr. R. Rivlin Bethlehem, PA 18015
1	Michigan State University College of Engineering ATTN: Prof. W. Sharpe East Lansing, MI 48823
1	New York University Department of Mathematics ATTN: Dr. J. Keller University Heights New York, NY 10053
1	North Carolina State University Department of Engineering Mechanics ATTN: Dr. W. Bingham Raleigh, NC 27607
1	Pennsylvania State University Engineering Mechanical Dept. ATTN: Prof. N. Davids University Park, PA 16502
1	Purdue University Institute for Mathematical Sciences ATTN: Dr. E. Cumberbatch Lafayette, IN 47907
2	Rice University ATTN: Dr. C. C. Wang Dr. R. Bowen P. O. Box 1892 Houston, TX 77001

DISTRIBUTION LIST

No. of Copies	Organization
1	Southern Methodist University Solid Mechanics Division ATTN: Prof. H. Watson Dallas, TX 75221
1	Temple University College of Engineering Tech. ATTN: Dr. R. Haythornthwaite Dean Philadelphia, PA 19122
1	The Johns Hopkins University ATTN: Prof. J. Bell 34th and Charles Streets Baltimore, MD 21218
1	Tulane University Dept of Mechanical Engineering ATTN: Dr. S. Cowin New Orleans, LA 70112
2	University of California ATTN: Dr. M. Carroll Dr. P. Naghdi Berkeley, CA [illegible]
1	University of California Dept of Aerospace and Mechanical Engineering Science ATTN: Dr. Y. C. Fung P. O. Box [illegible] La Jolla, CA [illegible]
1	University of California Department of Mechanics ATTN: Dr. P. Stern 504 Hilgard Avenue Los Angeles, CA [illegible]
1	University of California at Los Angeles Dept of Mechanics ATTN: W. Goldsmith Los Angeles CA [illegible]
1	University of Delaware Dept of Mechanical Engineering ATTN: Prof. J. Vinson Newark, DE 19711
3	University of Florida Dept. of Engineering Science and Mechanics ATTN: Dr. C. A. Sciammarilla Dr. L. Malvern Dr. E. Walsh Gainesville, FL 32601
2	University of Houston Department of Mechanical Engineering ATTN: Dr. T. Wheeler Dr. P. Naghdinger Houston, TX [illegible]
1	University of Illinois Dept. of Theoretical and Applied Mechanics ATTN: Dr. I. Carlson Urbana, IL [illegible]
1	University of Illinois Urbana Campus College of Engineering Dept. of Materials Engineering ATTN: [illegible] [illegible] P. O. Box [illegible] Urbana, IL [illegible]
1	University of Iowa ATTN: [illegible] Iowa City, IA [illegible]
1	University of Kentucky Dept. of Engineering Mechanics ATTN: Dr. M. Beatty [illegible] [illegible] [illegible] Lexington, KY [illegible]

DISTRIBUTION LIST

No. of Copies	Organization
2	University of Maryland Department of Mechanical Engineering ATTN: Prof. J. Yang Prof. J. Dally College Park, MD 20742
1	University of Minnesota Dept. of Engineering Mechanics ATTN: Dr. R. Fosdick Minneapolis, MN 55455
1	University of Notre Dame Department of Metallurgical Engineering and Materials Sciences ATTN: Dr. N. Brown Notre Dame, IN [illegible]
3	Washington State University Department of Physics ATTN: Prof. R. Fowles Prof. G. Duvall Prof. Y. Gupta Pullman, WA 99163
	Aberdeen Proving Ground
	Dir, USAMSAA ATTN: AMXSY-D AMXSY-MP, H. Cohen
	Cdr, USATECOM ATTN: AMSTE-TO-F
	Cdr, CRDC, AMCCOM ATTN: SMCCR-RSP-A SMCCR-MU SMCCR-SPS-IL

END

4-87

DTIC